Draft version September 29, 2019
Typeset using LaTeX **preprint** style in AASTeX62

Probing UV Photochemical Pathways for CN & HCN Formation in Protoplanetary Disks with the *Hubble Space Telescope*

Nicole Arulanantham,[1] Kevin France,[1] Paolo Cazzoletti,[2] Anna Miotello,[3] Carlo F. Manara,[3] P. Christian Schneider,[4] and Keri Hoadley[5]

[1]*Laboratory for Atmospheric and Space Physics, University of Colorado, 392 UCB, Boulder, CO 80303, USA*
[2]*Max-Planck-Institute for Extraterrestrial Physics (MPE), Giessenbachstr. 1, 85748, Garching, Germany*
[3]*European Southern Observatory, Karl-Schwarzschild-Str. 2, D-85748 Garching bei München, Germany*
[4]*Hamburger Sternwarte, Gojenbergsweg 112, 21029 Hamburg, Germany*
[5]*Department of Astronomy, California Institute of Technology, 1200 East California Blvd., Pasadena, CA 91125, USA*

ABSTRACT

The UV radiation field is a critical regulator of photochemical reactions at the surface of molecular gas disks around young stars. In an effort to understand the relationship between observed UV properties and infrared and sub-mm gas distributions, we present a joint analysis of new and archival *HST*, *Spitzer*, and ALMA/IRAM data for five young stars in the Lupus cloud complex and 14 systems in Taurus-Auriga. The *HST* spectra were used to measure Lyα and FUV continuum fluxes reaching the disk surface, which are both responsible for dissociating relevant molecular species (e.g. HCN, N_2). Semi-forbidden C II] λ2325 and UV-fluorescent H_2 emission were also measured, providing constraints on the inner disk populations of C^+ and vibrationally excited H_2 (H_2^*). We find a statistically significant positive correlation between 14 μm HCN emission and relative fluxes from the FUV continuum and C II] λ2325, consistent with model predictions that require N_2 photodissociation and carbon ionization to trigger the main CN/HCN formation pathways. We also report tentative evidence of a negative correlation between HCN and fractional Lyα emission, although we note that this result is strongly influenced by systematic uncertainties in the reconstruction method used to measure the Lyα fluxes. No clear relationships are detected between sub-mm CN and Lyα or FUV continuum emission, and neither CN or HCN shows any correlation with the UV-H_2. This is attributed to the spatial locations of the various molecular species, which span several vertical layers within the inner disk and radii across both the inner and outer disk. We expect that future observations with *JWST* will build on the picture of inner disk photochemistry presented here by enabling more sensitive surveys of IR molecular features at higher resolution than *Spitzer*.

Keywords: stars: pre-main sequence, protoplanetary disks, molecules

1. INTRODUCTION

Multi-wavelength observations of gas- and dust-rich disks around young stars have allowed us to start mapping the composition and structure of planet-forming material. Infrared surveys with *Spitzer* (Öberg et al. 2008; Pontoppidan et al. 2010; Bottinelli et al. 2010; Salyk et al. 2011b; Pascucci

et al. 2013) and *Herschel* (Dent et al. 2013) provided important constraints on warm molecular gas in surface layers of the inner disks ($r < 10\,\mathrm{AU}$), contributing column densities and temperatures of critical molecular gas species (e.g. H_2O, CO_2). Sub-mm observations of star-forming regions with the SMA and ALMA have revealed the structure of cold gas in the outer disks with unprecedented sensitivity and angular resolution, showing statistically significant trends in mass and radial extent as a function of age and formation conditions (Ansdell et al. 2016, 2017; Miotello et al. 2017; Tazzari et al. 2017; van Terwisga et al. 2019; Cazzoletti et al. 2019). Both observational and theoretical work demonstrates that the chemical evolution of molecular gas is strongly dependent on the ultraviolet radiation field reaching the surface of the disk (Walsh et al. 2012, 2015; Cazzoletti et al. 2018; Bergner et al. 2019; Miotello et al. 2019). However, the effects of disk geometry and varying UV flux are degenerate in physical-chemical models of the gas distributions, making it difficult to trace the precise locations of critical species within the disk in the absence of high resolution datasets.

Observational constraints on the UV flux reaching the disk surface are available from *HST* surveys of young stars with circumstellar disks (see e.g. Yang et al. 2012; France et al. 2012, 2014). The wavelength range available with the Cosmic Origins Spectrograph (*HST*-COS) includes Lyα emission ($\lambda = 1215.67\,\text{Å}$) and extends down to the FUV continuum ($\lambda = 912 - 1100\,\text{Å}$), providing estimates of key photochemical ingredients in the molecular gas disk (Bergin et al. 2003; Li et al. 2013). In addition to these direct tracers of the UV radiation field, emission lines from electronic transitions of H_2 are also detected in *HST*-COS and *HST*-STIS spectra (Herczeg et al. 2002, 2004; France et al. 2012). These features originate in surface layers close to the star (Hoadley et al. 2015), providing an independent way to estimate the UV flux reaching the innermost regions of the disk (Schindhelm et al. 2012b).

In this work, we present new and archival *HST*-COS and *HST*-STIS observations of a sample of five young systems in the ∼3 Myr Lupus complex. We interpret our measurements of the UV radiation field and molecular gas features in the context of sub-mm CN observations and HCN emission from *Spitzer*, including disks in Taurus-Auriga for comparison. We focus on these two molecules because their physical distributions are known to have a strong dependence on the UV radiation field (Cazzoletti et al. 2018; Bergner et al. 2019). Understanding their morphologies can therefore constrain abundances of volatile elements (C, N, and H) in regions where gas-phase oxygen may be depleted and emission from ^{12}CO, the second most abundant gas component, is fainter than expected (Miotello et al. 2017; Schwarz et al. 2018). The radial distributions of these molecules can then inform us about the composition of material available for in situ planetary accretion, setting important initial conditions for atmospheric chemistry (see e.g. Madhusudhan et al. 2011). To this end, we discuss the relationships between spectral tracers of the UV radiation field and integrated fluxes from CN and HCN, with particular consideration given to the impact of disk geometry and optical thickness of the molecular gas.

2. TARGETS & OBSERVATIONS

2.1. *A Sample of Young Disks in the Lupus Complex*

Our sample consists of five young stars with circumstellar disks in the nearby ($d \sim 150\,\mathrm{pc}$) Lupus cloud complex: RY Lupi, RU Lupi, MY Lupi, Sz 68, and J16083070. Table 1 lists the properties of each target, including stellar mass, disk inclination, and visual extinction (A_V). A_V is low along the line of sight to the Lupus clouds (Alcalá et al. 2017), making the region well-suited for UV

observations. This group of young systems shows a broad range of outer disk morphologies in ALMA observations of their gas and dust distributions. Two targets (RY Lupi, J16083070) are identified as transition disks (van der Marel et al. 2018), with inner dust cavity radii of 50, and 75 AU, respectively. RY Lupi appears to have a gas- and dust-rich inner disk as well, indicating that the clearing of material seen inside 50 AU is a gap, rather than a cavity (Arulanantham et al. 2018; van der Marel et al. 2018). RU Lupi and MY Lupi were observed at high resolution (∼5 AU) with ALMA as part of the Disk Substructures at High Angular Resolution Project (DSHARP; Andrews et al. 2018), which revealed multiple rings of 1.25 mm continuum emission within each disk (Huang et al. 2018). Sz 68, a triple system that was also included in DSHARP (Andrews et al. 2018), consists of a close binary and a distant third companion. The *HST* and ALMA observations presented here include emission from both binary components. However, the disk around the secondary star (component B) is much smaller and fainter than the circumprimary disk ($I_{peak,B}/I_{peak,A} = 0.23$; Kurtovic et al. 2018), indicating that the bulk of the UV emission comes from the primary component.

These systems were selected for follow-up with *HST* after a large ALMA survey of the Lupus clouds identified them as hosts to some of the most massive dust disks in the region (Ansdell et al. 2016, 2018). However, physical-chemical models of the ^{13}CO and C^{18}O emission demonstrate that the total gas masses are unexpectedly low (Miotello et al. 2017), which can be attributed to either shorter timescales than predicted for removing gas from the disk (e.g. via photoevaporation) or chemical pathways that trap carbon in larger molecules with higher freeze-out temperatures. Since UV photons are critical regulators of chemical processes in disk environments (see e.g. Bergin et al. 2003; Bethell & Bergin 2011; Walsh et al. 2012, 2015; Cazzoletti et al. 2018; Visser et al. 2018), the *HST* data we present here provide currently missing observational constraints on the levels of irradiation at the surface of the gas disk.

2.2. *Observations*

All five systems were observed with the *Hubble Space Telescope (HST)*, using both the Cosmic Origins Spectrograph (COS; Green et al. 2012) and the Space Telescope Imaging Spectrograph (STIS; Woodgate et al. 1997a,b). Table 2 lists exposure times and program IDs for the observations. The spectra for three of our targets were previously presented in France et al. 2012 (RU Lupi), Arulanantham et al. 2018 (RY Lupi), and Alcala' et al. 2019 (MY Lupi).

Five different modes of *HST*-COS and *HST*-STIS were used to observe four of our systems, providing wavelength coverage from 1100-5000 Å. We note that NUV coverage is not included for RU Lupi, which was observed as part of a different program. These data were used to extrapolate the FUV continuum down to 912 Å, which is a critical region for disk photochemistry but not readily accessible with available UV facilities (France et al. 2014). All five spectral modes were then stitched together to produce a SED for each system using the methods outlined in France et al. (2014) and Arulanantham et al. (2018). Figure 1 shows an overview of the SEDs, highlighting the strong contribution from the accretion-dominated NUV continuum $(\lambda \sim 3000 - 4000$ Å$)$. Accretion processes enhance the FUV continuum as well, but the total flux at $\lambda < 2000$ Å is dominated by line emission from hot, atomic gas (e.g. Lyα, C IV, C II, Mg II). Our resulting library of radiation fields, which encompasses far-ultraviolet to optical wavelengths, is available to the community. We anticipate that the data will be used in photochemical modeling efforts that require an understanding of stellar irradiation at the disk surface.

Sub-mm CN fluxes for this work were taken from the literature (Öberg et al. 2011; Guilloteau et al. 2013; van Terwisga et al. 2019), but HCN features were measured directly from observations with the InfraRed Spectrograph (IRS) onboard the *Spitzer Space Telescope* (Houck et al. 2004). All targets except J16083070 were observed in the high-resolution mode ($R \sim 600$) over the course of several different observing programs. The data were retrieved from the Combined Atlas of Sources with Spitzer IRS Spectra (CASSIS; Lebouteiller et al. 2011, 2015), which provides a complete catalog of *Spitzer*/IRS observations. Fluxes from the 14 μm HCN $v = 2$ band were measured over the wavelength range defined for the feature in Najita et al. (2013). That work used slab models of the molecular gas disk to identify line-free spectral windows for each target, which we used as a reference for continuum subtraction. The observing program IDs, PIs, and measured HCN fluxes are provided in Table 3.

2.3. *Archival* HST *Data from YSOs in Taurus-Auriga*

To increase the sample size of this study and compare properties between different star-forming regions, we include all Taurus-Auriga sources from the literature with both sub-mm CN fluxes and UV spectra from *HST*-STIS and/or *HST*-COS. Disks in Taurus are roughly equivalent in age to the Lupus systems (∼1-2 Myr vs. ∼1-3 Myr) and have similar dust mass distributions (Ansdell et al. 2016), making it easier to isolate the impact of the UV radiation field on the molecular gas distributions. The UV observations were carried out as part of two COS Guaranteed Time programs (PI: J. Green; PIDs: 11533, 12036) and The Disks, Accretion, and Outflows (DAO) of T Tau stars program (PI: G. Herczeg; PID: 11616). *HST*-COS observations were acquired with both the G130M and G160M gratings for all systems, providing wavelength coverage over the same range of FUV wavelengths (∼1100-1700 Å) as the spectra obtained for the five Lupus disks. Spectral features from these data (e.g. emission line strengths, accretion rates) have previously been analyzed in a number of papers, including Yang et al. (2012), Ardila et al. (2013), France et al. (2011, 2012, 2014, 2017), and references therein. We mirror the techniques described in those works to identify various properties in the new Lupus spectra, reporting uniform measurements over the entire Lupus/Taurus-Auriga disk sample.

2.4. *Uncertainty in Literature Measurements of* A_V

Observations at FUV wavelengths are highly affected by the amount of dust and gas along the line of sight to a disk (A_V), making accurate reddening corrections critical in interpreting the spectral features. France et al. (2017) report a statistically significant positive correlation between A_V (derived from e.g. broadband color excesses, deviations from stellar photospheric templates; Kenyon & Hartmann 1995; Hartigan & Kenyon 2003) and the total luminosity from UV-fluorescent H_2. The trend implies that more molecular gas emission is seen from disks with more intervening material; however, there is no physical or chemical process that would produce such a relationship between circumstellar and interstellar material, making systematic uncertainties in the A_V measurements a more likely driver. This effect must be removed in order to accurately assess relationships between the UV spectral features.

To get a less biased estimate of the optical extinction, McJunkin et al. (2014) used observed Lyα profiles to directly measure the amount of neutral hydrogen (H I) along the line of sight. A_V values were then calculated as $A_V/R_V = N(HI)/\left(4.8 \times 10^{21} \text{ atoms cm}^{-2} \text{ mag}^{-1}\right)$ (Bohlin et al. 1978). Extinctions derived using this method are typically significantly lower than reported in the literature,

and France et al. (2017) find that the correlation between A_V and $L(H_2)$ becomes statistically insignificant. Figure 3 compares the Lyα and FUV continuum luminosities calculated with $N(HI)$-based A_V values to the measurements using more traditional methods to estimate A_V, showing that the former yields much lower luminosities than the latter. Based on the results of McJunkin et al. (2014) and France et al. (2017), we adopt the H I-derived A_V values for the analysis presented here. We also normalize the UV luminosities of individual features (e.g. Lyα, UV-H_2) by the total UV luminosity, which further reduces the impact of systematic uncertainties in measuring A_V.

3. RESULTS

The *HST*-COS and *HST*-STIS spectra described above provide direct measurements of the UV radiation field, which we use to estimate the UV flux reaching the surface of the gas disk. Here we focus on the role of UV photons in producing CN, which has been detected in ALMA Band 7 observations of a large sample of disks in the Lupus clouds (van Terwisga et al. 2019), including the five studied here. We present the following results under the assumption that the dominant reaction pathway for CN production in disks is

$$\begin{aligned} N + H_2^* &\longrightarrow NH + H \\ C^+ + NH &\longrightarrow CN^+ + H \\ CN^+ + H &\longrightarrow CN + H^+, \end{aligned} \tag{1}$$

where H_2^* is vibrationally excited H_2 (Walsh et al. 2015; Cazzoletti et al. 2018). HCN can then be formed via reactions with H_2 and CH_4

$$\begin{aligned} CN + H_2 &\longrightarrow HCN + H \\ CN + CH_4 &\longrightarrow HCN + CH_3 \end{aligned} \tag{2}$$

(Baulch et al. 1994; Walsh et al. 2015). Destruction of HCN by UV photons also contributes significantly to the total abundance of CN in the disk, with photodissociation occurring at a rate of 1.6×10^{-9} s^{-1} under a typical interstellar radiation field (van Dishoeck et al. 2006; Walsh et al. 2015; Cazzoletti et al. 2018).

While the Lupus ALMA survey measured fluxes from the $N = 3-2$ hyperfine CN transitions (van Terwisga et al. 2019), measurements of CN emission from the literature report $N = 2-1$ fluxes for targets in other young associations (Guilloteau et al. 2013; Öberg et al. 2011). To convert the fluxes from different datasets to comparable quantities, we adopted the methodology of van Terwisga et al. (2019) and used the ratio

$$\frac{N = 2-1, J = 5/2-3/2}{N = 3-2, J = 7/2-5/2} = 1.6 \tag{3}$$

to obtain CN $N = 3-2$ flux estimates for the remaining disks. This scaling accounts for the gas temperature distribution within the disk, under the assumption that the CN emission is optically thin. The value chosen by van Terwisga et al. (2019) (which we use here) is the median from the grid of models studied by Cazzoletti et al. (2018).

3.1. *Photodissociation of N_2 by the FUV Continuum*

Photochemical models of protoplanetary disks find that column densities of nitrogen-dependent molecular species (e.g. CN, HCN) vary with the total FUV flux at the disk surface (Pascucci et al.

2009; Walsh et al. 2012, 2015). The trend is attributed to photoabsorption, since five excited electronic transitions of N_2 fall between 912-1100 Å. Absorption at these wavelengths produces pre-dissociated N_2^* via coupling to the continuum (Li et al. 2013). As shown in Eq. 1, the atomic nitrogen products react with H_2^* to produce NH in regions where gas temperatures are at least 1500-2500 K (Baulch et al. 2005), therefore catalyzing formation of molecules like CN and HCN (Walsh et al. 2015).

The predicted relationship between molecular abundances and UV irradiation is corroborated by observational studies at IR wavelengths, which find that disks around cool M stars show less emission from nitrogen bearing molecules than disks around hotter solar-type stars (Pascucci et al. 2009, 2013; Najita et al. 2013). The difference is attributed to varying UV photon production rates, which are expected to be lower in cooler stars (Walsh et al. 2012, 2015). To further investigate this relationship from an observational perspective, we compare CN fluxes measured from ALMA observations (van Terwisga et al. 2019) to FUV fluxes from the *HST*-COS and *HST*-STIS spectra presented here.

Although our *HST* data is truncated below 1000 Å, the method from France et al. (2014) was used to make robust estimates of the FUV continuum at shorter wavelengths. The extrapolation was performed on binned fluxes, which were calculated in 210 line-free regions from the longer wavelength data. The continua were fitted with a second order polynomial and extended down to 912 Å. For uniformity with the larger sample presented in France et al. (2014), we report the total integrated flux from wavelengths <1650 Å and compare these FUV continuum luminosities to both CN and HCN emission (see Figure 5). We find a significant postive correlation between the FUV and HCN fluxes ($\rho = 0.62; p = 0.01$), implying that the inner disk population of HCN is enhanced in systems with more FUV radiation relative to the rest of the UV spectrum. However, we find no significant trends between the FUV and CN fluxes ($\rho = -0.2; p = 0.3$). We explore this inconsistency further in Section 4.

3.2. *Lyα as a Regulator of Disk Chemistry*

Lyα emission is by far the strongest component of the UV radiation field, comprising roughly 75-95% of the total flux from $\sim 912 - 1700$ Å (Bergin et al. 2003; Herczeg et al. 2004; Schindhelm et al. 2012b; France et al. 2014). Its broad width in wavelength space encompasses transitions of a variety of molecules, including electronic transitions of H_2 (Herczeg et al. 2002, 2004) and CO (France et al. 2011; Schindhelm et al. 2012a) and photodissociation energies of HCN, C_2H_2 (Bergin et al. 2003; Walsh et al. 2015), and H_2O (France et al. 2017). However, the observed Lyα feature is always contaminated by geocoronal emission and ISM absorption along the line-of-sight, making direct measurements difficult. Instead, we use the method from Schindhelm et al. (2012b) to reconstruct the Lyα profiles for the five Lupus disks from observations of UV-fluorescent H_2.

UV-H_2 fluorescence is activated when a population of hot, vibrationally excited H_2 ($T > 1500$ K; Ádámkovics et al. 2016) is pumped into excited electronic states by photons with energies that fall along the Lyα line profile (Herczeg et al. 2002, 2004). A cascade of UV emission lines is then observed as the gas transitions back to the ground electronic state. The features can be divided into groups called progressions, where a single progression, denoted $[\nu', J']$, consists of all transitions out of the same upper level with vibrational state ν' and rotational state J' (Herczeg et al. 2002, 2004). We measured fluxes from the strongest emission lines in 12 progressions (see Table 2 of France et al. 2012) by integrating over models of a Gaussian profile convolved with the *HST*-COS line-spread function (LSF) and superimposed on a linear continuum. Upper limits on features indistinguishable from the continuum were calculated as the RMS flux within a 3 Å range across the expected line

center. The total fluxes were then used as Lyα "data" (y), where the x value for each data point is the Lyα pumping wavelength for the electronic transition. We then fit a model Lyα profile to the $(x_i, y_i) = (\lambda_{LyA,i}, F_{H_2,i})$ data points.

The Lyα model consists of an initial "intrinsic" Gaussian emission line, an H I outflow between the star/accretion shock and the molecular gas disk, and a population of hot H_2 that absorbs the Lyα photons. We allow five model parameters to vary: the amplitude of the intrinsic profile ($I_{Ly\alpha}$), the velocity and column density of the outflowing H I (v_{out}, N_{out}), and the temperature and column density of the absorbing H_2 (T_{H_2}, N_{H_2}). The FWHM of the intrinsic profile for each system was fixed to the average, maximum, and minimum values from Schindhelm et al. (2012b), resulting in three model profiles for each target. Posterior distributions for the model parameters were constructed using MCMC sampling (Foreman-Mackey et al. 2013) within the bounds defined by Schindhelm et al. (2012b). However, we find that the model uncertainties are better captured by the variations in the average, maximum, and minimum FWHM profiles. Figure 6 shows the median Lyα profile at the disk surface for all five Lupus systems, with colored contours representing the bounds set by the three FWHM values.

We compare the total luminosities from our reconstructed Lyα profiles to the ALMA CN luminosities from van Terwisga et al. (2019) (see Figure 8). Since CN molecules can also form as byproducts of HCN or CH_3CN photodissociation (Walsh et al. 2015) via Lyα photons at 1216.3 Å and 1217.8 Å, respectively (Nuth & Glicker 1982; Bergin et al. 2003), we expect that increased Lyα irradiation of the disk surface will increase the significance of dissociative pathways in regulating both CN and HCN column densities. In agreement with model predictions, we find a statistically significant negative correlation between the normalized Lyα and HCN luminosities ($\rho = -0.5; p = 0.04$), implying that inner disk HCN is more readily photodissociated in systems with more Lyα flux relative to the rest of the UV spectrum. As with the FUV continuum, we find no significant linear relationship between the reconstructed Lyα and CN emission (Spearman $\rho = 0.45$; $p = 0.09$).

Since the Lyα profiles are derived from UV-fluorescent H_2^*, the lack of correlation between CN and Lyα emission may be attributed to the difference in vertical distributions of the two molecules. Cazzoletti et al. (2018) find that H_2^* is expected to survive from ∼0-100 AU above the disk midplane, while CN is only present between ∼25-75 AU. Since the UV-H_2 emission likely originates from the disk surface, a direct comparison between observed Lyα and CN luminosities likely requires more careful treatment of optical depth effects. We also note that the uncertainties in the reconstructed Lyα profiles are large enough to mask any underlying relationship between the fluxes presented in Figure 8.

3.3. *Mapping the population of H_2^**

3.3.1. *Lyα-pumped H_2*

As introduced in Section 3.1.3, we detect a suite of emission lines from hot ($T \sim 1500 - 2500$ K; Ádámkovics et al. 2016), fluorescent H_2 in the *HST*-COS spectra of all five disks. The features originate from a population of vibrationally excited gas (H_2^*), which can be "pumped" from the ground electronic state $\left(X^1\Sigma_g^+\right)$ into the first excited electronic state ($B^1\Sigma_u^+$) by Lyα photons. Fluorescent UV emission lines are then produced as the molecules transition back to the ground electronic state (Herczeg et al. 2002, 2004). Although our *HST*-COS spectra are not spatially resolved, *HST*-STIS spectra of the same features in the disk around TW Hya showed that the H_2 emission must be within

$\sim$2 AU of the central star (Herczeg et al. 2004). The features may therefore provide constraints on the distribution of H_2^* available for CN and HCN formation in the inner disk region. Figure 9 provides a cartoon demonstrating the rough spatial locations of the emitting gas.

The UV-H_2 emission lines are spectrally resolved (i.e. broader than the *HST*-COS resolution), allowing us to extract information about the spatial distribution of hot, fluorescent gas. Assuming that the material is in a Keplerian disk, the FWHMs of the emission lines can be mapped to an average radial location as

$$\langle R_{H_2} \rangle = GM_* \left(\frac{2 \sin i}{FWHM} \right)^2 \tag{4}$$

(Salyk et al. 2011a; France et al. 2012), where M_* is the stellar mass and i is the disk inclination. We average the FWHMs of the strongest emission lines from the $[\nu', J'] = [1,4]$, $[1,7]$, $[0,1]$, and $[0,2]$ progressions and calculate a radius for each progression (see Table 5). Although resonant scattering should allow pumping photons from the Lyα line wings to penetrate deeper into the disk than those from the line center (Bethell & Bergin 2011), we find no trends between pumping wavelength and average emitting radius.

Since H_2^* is required to produce CN (see Eq. 1), the UV-H_2 features are a probe of the uppermost layer of available reactants at the average radial location of emitting gas (R_{H_2}). We explore this relationship by comparing the CN and HCN luminosities to the total flux from fluorescent UV-H_2 emission lines (see Figure 11), finding that neither species is correlated with the UV-H_2. This can be attributed to the same vertical stratification effects discussed in Section 3.2, since the three molecules are expected to peak at different heights relative to the disk midplane (Cazzoletti et al. 2018). Since Lyα photons are only able to pump H_2^* in a thin surface layer, the UV-H_2 features do not contain information from vibrationally excited gas present deeper in the disk. However, the radial distribution of UV-H_2 can provide direct measurements of how far Lyα emission is expected to travel. We use 2-D radiative transfer models of the features to constrain the UV irradiation at the disk surface in Section 4.

3.3.2. *1600 Å "Bump" as a Signature of H_2O Dissociation*

Previous studies of UV continuum emission from young stars with disks have identified an excess "bump" in the spectra around $\sim$1600 Å (Herczeg et al. 2004; Bergin et al. 2004). The feature is attributed to continuum and line emission from vibrationally excited H_2, produced when Lyα photons dissociate H_2O in the inner disk ($r < 2$ AU; France et al. 2017). While the Lyα and bump luminosities are strongly correlated ($\rho = 0.74$, $p = 1.72 \times 10^{-3}$; France et al. 2017), no relationship is observed between the bump and X-ray luminosities (Espaillat et al. 2019). This implies that Lyα photons may play a more prominent role than the X-ray radiation field in regulating the distribution of hot H_2O and vibrationally excited H_2 at radii close to the central star.

We use the method described in France et al. (2017) to measure bump fluxes and calculate luminosities for the three disks in our sample that were not included in that work. A second order polynomial fit to the FUV continuum, representative of the underlying flux, was integrated from 1490-1690 Å and subtracted from the total observed flux in the same wavelength region. The residual flux can be attributed to the bump alone (see Table 4). Figure 13 compares the CN/HCN and bump luminosities, again showing no clear linear trend between the spectral features. The H_2^* responsible for producing the bump is therefore likely located closer to the disk surface than the inner disk populations of CN and HCN.

3.4. *C II] λ2325 Emission as a Tracer of Inner Disk C^+*

The semi-forbidden C II] λ2325 emission line is detected in all the Lupus and Taurus-Auriga targets with *HST*-STIS spectra. Models of the feature in other young systems find that its shape is consistent with an origin at the base of a warm, inner disk ($r \sim 0.1 - 1$ AU) wind, coincident with surface layers of the disk itself (Gómez de Castro & Ferro-Fontán 2005) and similar to the [O I] 6300 Å line (Simon et al. 2016). Studies of the [O I] line show that the profile becomes narrower as dust is removed from the inner disk (Banzatti et al. 2019), implying that the base of the wind, and therefore all the emitting gas it contains, shifts to more distant radii with the disk itself. If the base of the disk wind is co-located with the surface layers of the inner disk, C II] may be an important observational proxy for the population of inner disk C^+. Ionized carbon (C^+) is a key reactant in the main formation pathways of C_2H (Henning et al. 2010; Walsh et al. 2015; Miotello et al. 2019) and CN (Walsh et al. 2015; Cazzoletti et al. 2018). C^+ also plays an important role in CO_2 destruction, with physical-chemical models showing an enhancement in the CO_2 column density at $r \sim 10$ AU, where gas self-shielding allows the C^+/C ratio to drop below unity (Walsh et al. 2012). We note that the FUV CII λ1335 resonant feature is also included in the datasets presented here. However, its corresponding population of C^+ is strongly correlated with accretion diagnostics (Calvet et al. 2004; Johns-Krull & Herczeg 2007) and does not necessarily trace material that is directly involved in molecule formation and destruction.

To explore whether the C II] emission is related to the CN and HCN observations, C II] line fluxes were measured for each target in our sample by fitting the dereddened *HST*-STIS spectra with a model Gaussian profile superimposed on a linear continuum (see Table 4). Figure 15 compares the CN, HCN, and C II] λ2325 luminosities, showing statistically significant relationships between the relative fluxes from C II] and emission from both molecular species. We find that HCN emission is stronger in systems with higher C II] fluxes ($\rho = 0.67; p = 0.015$), although CN emission appears to decline as C II] fluxes increase ($\rho = -0.6; p = 0.01$). However, we note that the CN relationship is largely driven by GM Aur and SU Aur, which both have high H-leverage values and studentized residuals when included in a linear regression model of the form $L_{CN} = m \times L_{CII]}/L_{UV,total} + b$.

In order to verify the spatial location of the C II] feature, we compare the measured widths of the C II] lines to the radial location of the innermost resolved sub-mm dust ring, gap, or cavity in Figure 16. We do not find any relationship between the two quantities, implying that the C II] does not trace the inner disk edge as closely as the [O I] λ6300 feature (Simon et al. 2016). Instead, the emission appears to come from a population of C^+ that is enhanced in systems with stronger FUV continuum emission (see Figure 17). Although C II] is not significantly correlated with the mass accretion rate ($\rho = 0.33; p = 0.26$), the relationship may still be a byproduct of accretion-related processes. Since only a handful of targets presented here have high-resolution *HST*-STIS observations of the C II] λ2325 feature, a more detailed kinematic analysis of the line properties is outside the scope of this work.

4. DISCUSSION

Physical-chemical models of disks have suggested that emission from Lyα and the FUV continuum is directly related to molecular gas abundances, providing photons at the energies required for photochemical reactions to proceed. Although we find significant correlations between both UV components and emission from 14 μm HCN, neither UV tracer appears to be related to the sub-mm

CN fluxes. Furthermore, the CN distributions are also not correlated with UV emission from Lyα-pumped H_2^* or semi-forbidden C II] emission from the inner disk C^+ population, both of which are ingredients for the main reaction pathway in CN formation. In order to understand this discrepancy, we examine the impact of disk geometry on the observed spectra and consider whether the optical thickness of the various emission lines has a significant impact on our results.

4.1. *Extent of UV-H_2 Emitting Region*

UV-H_2 emission is generally confined to the inner disk, although several systems (e.g. RU Lupi) show line profiles with prominent blue wings, consistent with emission from an outflow (Herczeg et al. 2005; France et al. 2012). Since the molecular gas is pumped by internal Lyα radiation from the star and accretion shock, the radial extent of the fluorescent region is limited by how far the pumping photons can travel into the disk (see e.g. (Hoadley et al. 2015)). The UV-H_2 emission is therefore only a tracer of the underlying H_2^* (and by extension, CN) distribution that is accessible to Lyα photons.

To investigate the radial limit of our UV-H_2 observations, we use the 2-D radiative transfer model developed by Hoadley et al. 2015 to reproduce the distributions of fluorescent gas in 4/5 of the Lupus disks presented here. The model propagates Lyα photons into a Keplerian disk with radially varying distributions of temperature,

$$T\left(r\right) = T_{1AU}\left(\frac{r}{1\,\mathrm{AU}}\right)^{-q} \tag{5}$$

pressure scale height,

$$H_p\left(r\right) = \sqrt{\frac{kT\left(r\right)}{\mu m_H}\frac{r^3}{GM_*}} \tag{6}$$

and surface density

$$\Sigma\left(r\right) = \Sigma_c\left(\frac{r}{r_c}\right)^{-\gamma}\exp\left[-\left(\frac{r}{r_c}\right)^{2-\gamma}\right] \tag{7}$$

at some height z above the disk midplane. We calculate the mass density distribution ($\rho\left(r,z\right)$) for the entire volume of H_2 gas and the corresponding number density $\left(n_{[\nu,J]}\left(r,z\right)\right)$ and optical depth ($\tau_\lambda\left(r,z\right)$) of molecules in the upper level of each progression. Once the physical structure of the underlying hot H_2 population has been derived, the distribution of UV-H_2 flux from each transition is calculated as

$$F_{\lambda_{H_2}}\left(r,z\right) = \eta F_{*,Ly\alpha}\left(\frac{R_*^2}{r^2}\right)\left(\frac{\left(r\cos i_{disk}\right)^2}{s\left(r,z\right)^2}\right)\times B_{mn}\Sigma^{\tau'_\lambda}\left(1-e^{-\tau'_\lambda(r,z)}\right) \tag{8}$$

The flux distribution is then summed over the entire disk, producing an emission line profile that we fit directly to the observed UV-H_2 spectra. The resulting model distribution of gas informs us about where in the disk the H_2^* is exposed to Lyα radiation, providing radial constraints on the uppermost layer of reactants for producing CN molecules in the inner disk.

Figure 19 shows the radial distributions of UV-H_2 flux that best reproduce the observed emission lines from the Lupus disks. The shapes of the gas distributions generally follow the sub-mm dust distributions, consistent with the results from Hoadley et al. (2015) that showed more distant UV-H_2 emitting regions in disks with dust gaps or cavities. Sz 68, which is a close binary (Ghez et al. 1997),

shows a distribution that is sharply truncated at 10 AU. This is consistent with UV-H_2 emission from the primary component alone (Kurtovic et al. 2018), with Lyα photons reaching the gas surface layers out to the circumprimary disk edge. MY Lupi, which has two shallow gaps at 8 and 20 AU (Huang et al. 2018), shows no sign of breaks in the gas disk at those radii, although the flux distribution declines rapidly from its peak at ∼0.25 AU. Finally, we report that the UV-H_2 emission in J16083070 extends out to ∼100 AU, with a flat distribution from ∼0.3-10 AU followed by a slow decline to the outer disk regions. This is consistent with the observed dust depletion inside of 75 AU (van der Marel et al. 2018), which allows UV photons to reach gas at more distant radii. However, we note that the outer radius of the UV-H_2 distribution is limited by the *HST*-COS spectral resolution $\left(\Delta v \sim 17 \text{ km s}^{-1}\right)$. Given the stellar mass and disk inclination of J16083070, this corresponds to a radius limit of ∼20 AU.

Although the UV-H_2 lines are unable to probe the bulk H_2^* population at the disk heights where CN is expected to form, the radial distributions of flux from hot, fluorescent gas provide constraints on where the disk surface becomes optically thick to Lyα photons. Figure 20 compares the outer radius of the UV-H_2 distribution, defined as the location which 95% of the total flux, to the CN luminosities, showing that systems with UV-H_2 emission extending to more distant radii generally have stronger luminosities. Although the correlation isn't quite statistically significant ($\rho = 0.55; p = 0.08$), the observed trend confirms the model prediction that CN formation pathways are significantly dependent on the UV radiation field. This relationship will be further explored in a future paper.

5. SUMMARY & CONCLUSIONS

We have analyzed the ultraviolet spectral properties of 19 young stars in the Lupus and Taurus-Auriga associations, using spectra from *HST*-COS and *HST*-STIS to directly measure fluxes from Lyα, the FUV continuum, semi-forbidden C II] λ2325, and UV-fluorescent H_2. Each of these is a potential tracer of the photochemical pathways responsible for producing CN and HCN molecules in disks. To investigate the formation chemistry of these two species, we compare the UV tracers to sub-mm CN and 14 μm HCN fluxes. We find that

1. HCN fluxes are positively correlated with relative fluxes from the FUV continuum and C II] λ2325, implying that disks with strong continuum fluxes are more readily able to produce the atomic N and C+ reactants required in the first step of the main HCN formation pathway.

2. HCN emission is negatively correlated with Lyα emission, consistent with model predictions that predict increased photodissociation with stronger Lyα irradiation.

3. CN emission and the outer radii of the UV-H_2 flux distributions are tentatively positively correlated, implying that CN formation is enhanced in systems that are optically thin to UV radiation out to more distant disk radii.

We attribute the lack of correlations between CN and HCN emission and UV-H_2 fluxes to the spatial distributions of the three molecular species, since the UV-H_2 is concentrated in surface layers of the inner disk, the sub-mm CN emission extends from the inner to the outer disk, and the HCN emission originates in deeper layers of the inner disk. By combining UV spectra with IR and sub-mm fluxes from UV-dependent molecular gas species, we are able to observationally confirm the significance of the main CN/HCN formation pathways in protoplanetary disks. The analysis presented here can be extended to additional species (e.g. hydrocarbons) in the era of *JWST*, which will enable higher

Table 1: Stellar & Disk Properties

Target	Distance [pc]	M_* [$M_\odot$]	A_V [mag]	i °	$r_{cav,dust}$ [AU]	$r_{cav,gas}$ [AU]	References
RU Lupi*	159	0.8	0.07	∼18.5°	14, 17, 21, 24, 29.1, 34, 42, 50	...	a b c
RY Lupi	158	1.47	0.1	68	50	50	a d
MY Lupi *	156	1.02	0.04	73	8, 20, 30, 40	25	a b d
Sz 68	154	2.13	0.15	34	...	...	a e
J16083070	155	1.81	0.055	74	75	60	a d

*High-resolution ALMA images of RU Lupi have revealed a series of rings inside ∼50 AU (Huang et al. 2018). The two rings with constrained values have inclinations of 20° and 17°, so we use an average of the two. For both RU Lupi and MY Lupi, the $r_{cav,dust}$ radii are locations of the dust rings resolved by (Huang et al. 2018).

[a] Bailer-Jones et al. 2018

[b] Huang et al. 2018

[c] van der Marel et al. 2018

[d] Ansdell et al. 2016

spectral resolution observations of warm molecular gas and more accurate physical-chemical models of surface reactions in planet-forming systems.

6. ACKNOWLEDGEMENTS

NA is supported by NASA Earth and Space Science Fellowship grant 80NSSC17K0531. This paper makes use of the following ALMA data: ADS/JAO.ALMA#2013.1.00220.S. ALMA is a partnership of ESO (representing its member states), NSF (USA) and NINS (Japan), together with NRC (Canada), MOST and ASIAA (Taiwan), and KASI (Republic of Korea), in cooperation with the Republic of Chile. The Joint ALMA Observatory is operated by ESO, AUI/NRAO and NAOJ. This work utilized the RMACC Summit supercomputer, which is supported by the National Science Foundation (awards ACI-1532235 and ACI-1532236), the University of Colorado Boulder, and Colorado State University. The Summit supercomputer is a joint effort of the University of Colorado Boulder and Colorado State University. This research made use of Astropy,[1] a community-developed core Python package for Astronomy (Astropy Collaboration et al. 2013; The Astropy Collaboration et al. 2018).

APPENDIX

A. UV-H_2 SPECTRA AND MODELING RESULTS

We present the nine strongest observed UV-H_2 emission lines for RU Lupi, MY Lupi, Sz 68, and J16083070, with "best-fit" models from the 2-D radiative transfer approach described in Section 4.2 overlaid on the data. The corresponding model radial distributions of UV-H_2 flux for each system, with contours representing $+/-1-\sigma$ bounds, are shown as well.

[1] http://www.astropy.org

Table 2: Observations of Young Systems in Lupus

	RU Lupi*	RY Lupi	MY Lupi	Sz 68	J16083070
Program ID	12036, 8157	14469	14604	14604	14604
			Exposure Times [s]		
***HST*-COS G140L** (λ1280; $R \sim 1500$)	···	2448	5658	5538	5574
***HST*-COS G130M** (λ1291; $R \sim 16000$)	1686	654	1242	1212	1218
***HST*-COS G160M** (λ1577; $R \sim 16000$)	1938	648	1296	1266	1278
***HST*-STIS G230L** (λ2375; $R \sim 1000$)	···	2400	2028	1968	1986
***HST*-STIS G430L** (λ4300; $R \sim 1000$)	120	60	60	60	60

∗The G160M λ1589 setting was used for RU Lupi instead of λ1577.

Table 3: *Spitzer*/IRS PIDs and Fluxes

Target	Program ID	PI	HCN Fluxes [10^{-14} erg s^{-1} cm^{-2}]
AA Tau	20363	J. Carr	4.02
BP Tau	20363	J. Carr	4.45
DE Tau	50641	J. Carr	2.22
DM Tau	30300	J. Najita	0.69
DN Tau	30300	J. Najita	3.41
DR Tau	50641	J. Carr	17.7
DS Tau	50498	J. Houck	6.15
GM Aur	30300	J. Najita	0.67
HN Tau A	50641	J. Carr	2.41
LkCa 15	40338	J. Najita	2.71
MY Lupi	20611	C. Wright	1.49
RU Lupi	172	N. Evans	7.95
RY Lupi	172	N. Evans	1.23
RY Tau	40113	F. Lahuis	9.33
SU Aur	50641	J. Carr	7.83
Sz 68	172	N. Evans	3.98
T Tau	40113	F. Lahuis	70.3
J16083070	···	···	···
V4046 Sgr	3580	M. Honda	3.55

Table 4: Hot Gas & Stellar Luminosities

Target	L_{H_2} [10^{30} erg s^{-1}]	$L_{1600\mathring{A}}$ [10^{29} erg s^{-1}]	$L_{Ly\alpha}$ [10^{29} erg s^{-1}]	$L_{CII]}$ [10^{29} erg s^{-1}]
RU Lupi	6.1 ± 0.4	5.54 ± 1.59[a]	170 ± 70	···
RY Lupi	1.01 ± 0.08	1.55 ± 0.8[a]	70 ± 25	0.284
MY Lupi	0.45 ± 0.04	15.3 ± 6	18[b]	0.0582
Sz 68	0.27 ± 0.03	3.1 ± 1	5[b]	0.8
J16083070	0.6 ± 0.1	1.7 ± 0.7	37[b]	···

[a] Values from France et al. (2017).

[b] Reconstructed Lyα profiles have large uncertainties, due to noisy UV-H_2 emission lines

Table 5: Average Emission Radii of Hot, Fluorescent H_2

Target	$FWHM_{[1,4]}$ [km/s]	$\langle R_{H_2} \rangle_{[1,4]}$ [AU]	$FWHM_{[1,7]}$ [km/s]	$\langle R_{H_2} \rangle_{[1,7]}$ [AU]	$FWHM_{[0,1]}$ [km/s]	$\langle R_{H_2} \rangle_{[0,1]}$ [AU]	$FWHM_{[0,2]}$ [km/s]	$\langle R_{H_2} \rangle_{[0,2]}$ [AU]
RU Lupi	51 ± 1	0.10 ± 0.03	49 ± 2	0.11 ± 0.03	31 ± 2	0.29 ± 0.08	50 ± 3	0.11 ± 0.03
RY Lupi*	53.3 ± 0.7	1.8 ± 0.5	51 ± 1	2.0 ± 0.5	63 ± 10	1 ± 1	45 ± 4	2.6 ± 0.8
MY Lupi	48 ± 1	1.4 ± 0.2	46 ± 2	1.5 ± 0.2	48 ± 1	1.4 ± 0.2	59 ± 3	0.9 ± 0.1
Sz 68	57 ± 2	0.5 ± 0.3	57 ± 5	0.5 ± 0.3	57 ± 5	0.5 ± 0.4	43 ± 3	0.8 ± 0.6
J16083070	47.1 ± 0.7	2 ± 1	42.5 ± 0.7	3 ± 2	77 ± 10	0.8 ± 0.4	75 ± 10	0.8 ± 0.4

* The FWHMs listed here for RY Lupi are from single-component fits to the emission lines. Arulanantham et al. (2018) presents a more detailed analysis of the H_2 line shapes, showing that the strongest features in the [1,4] progression are better fit by a two-component model. We also adopt the disk inclination from van der Marel et al. (2018) (68°), instead of the scattered light inclination from Manset et al. (2009) (85.6°).

REFERENCES

Ádámkovics, M., Najita, J. R., & Glassgold, A. E. 2016, ApJ, 817, 82

Alcala', J. M., Manara, C. F., France, K., Schneider, C. P., Arulanantham, N., Miotello, A., Guenther, H. M., & Brown, A. 2019, arXiv e-prints

Alcalá, J. M., et al. 2017, A&A, 600, A20

Andrews, S. M., et al. 2018, ApJL, 869, L41

Ansdell, M., Williams, J. P., Manara, C. F., Miotello, A., Facchini, S., van der Marel, N., Testi, L., & van Dishoeck, E. F. 2017, AJ, 153, 240

Ansdell, M., et al. 2018, ApJ, 859, 21

—. 2016, ApJ, 828, 46

Ardila, D. R., et al. 2013, ApJS, 207, 1

Arulanantham, N., et al. 2018, ApJ, 855, 98

Astropy Collaboration et al. 2013, A&A, 558, A33

Bailer-Jones, C. A. L., Rybizki, J., Fouesneau, M., Mantelet, G., & Andrae, R. 2018, AJ, 156, 58

Banzatti, A., Pascucci, I., Edwards, S., Fang, M., Gorti, U., & Flock, M. 2019, ApJ, 870, 76

Baulch, D. L., et al. 2005, Journal of Physical and Chemical Reference Data, 34, 757

—. 1994, Journal of Physical and Chemical Reference Data, 23, 847

Bergin, E., Calvet, N., D'Alessio, P., & Herczeg, G. J. 2003, ApJL, 591, L159

Bergin, E., et al. 2004, ApJL, 614, L133

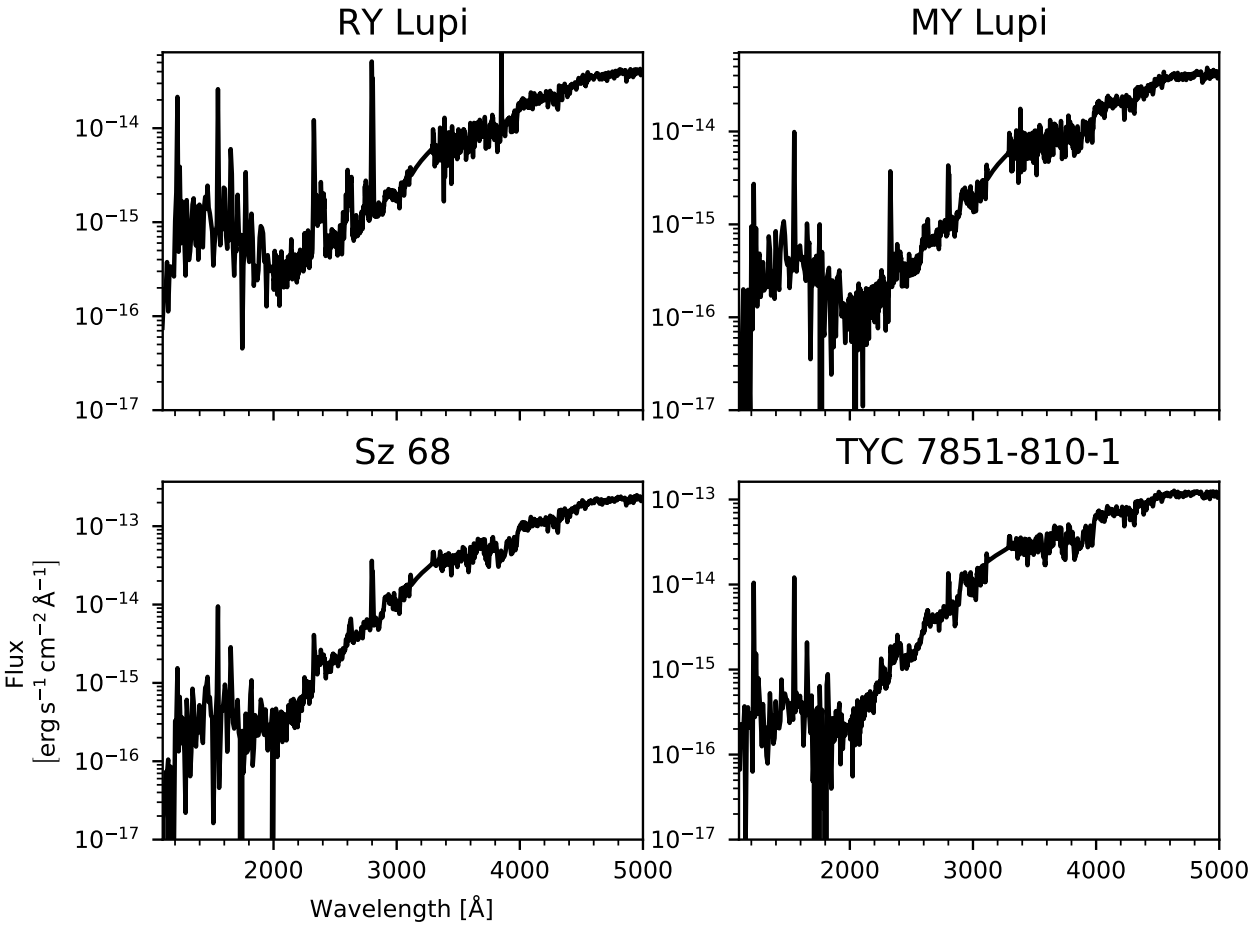

Figure 1: A panchromatic spectrum was produced for four disks in Lupus by stitching together new data from five different observing modes of *HST*-COS and *HST*-STIS. We include reconstructed model Lyα profiles (see e.g. Schindhelm et al. 2012b) in place of the observed features, which are contaminated by interstellar absorption and geocoronal emission. The spectra from RU Lupi and the disks in Taurus-Auriga were previously presented in Herczeg et al. (2005) and France et al. (2014).

Bergner, J. B., Öberg, K. I., Bergin, E. A., Loomis, R. A., Pegues, J., & Qi, C. 2019, ApJ, 876, 25
Bethell, T. J., & Bergin, E. A. 2011, ApJ, 739, 78
Bohlin, R. C., Savage, B. D., & Drake, J. F. 1978, ApJ, 224, 132
Bottinelli, S., et al. 2010, ApJ, 718, 1100
Calvet, N., Muzerolle, J., Briceño, C., Hernández, J., Hartmann, L., Saucedo, J. L., & Gordon, K. D. 2004, AJ, 128, 1294
Cazzoletti, P., et al. 2019, arXiv e-prints
Cazzoletti, P., van Dishoeck, E. F., Visser, R., Facchini, S., & Bruderer, S. 2018, A&A, 609, A93
Dent, W. R. F., et al. 2013, PASP, 125, 477
Espaillat, C. C., Robinson, C., Grant, S., & Reynolds, M. 2019, arXiv e-prints
Foreman-Mackey, D., Hogg, D. W., Lang, D., & Goodman, J. 2013, PASP, 125, 306
France, K., Roueff, E., & Abgrall, H. 2017, ApJ, 844, 169
France, K., Schindhelm, E., Bergin, E. A., Roueff, E., & Abgrall, H. 2014, ApJ, 784, 127
France, K., et al. 2011, ApJ, 734, 31
—. 2012, ApJ, 756, 171
Ghez, A. M., McCarthy, D. W., Patience, J. L., & Beck, T. L. 1997, ApJ, 481, 378

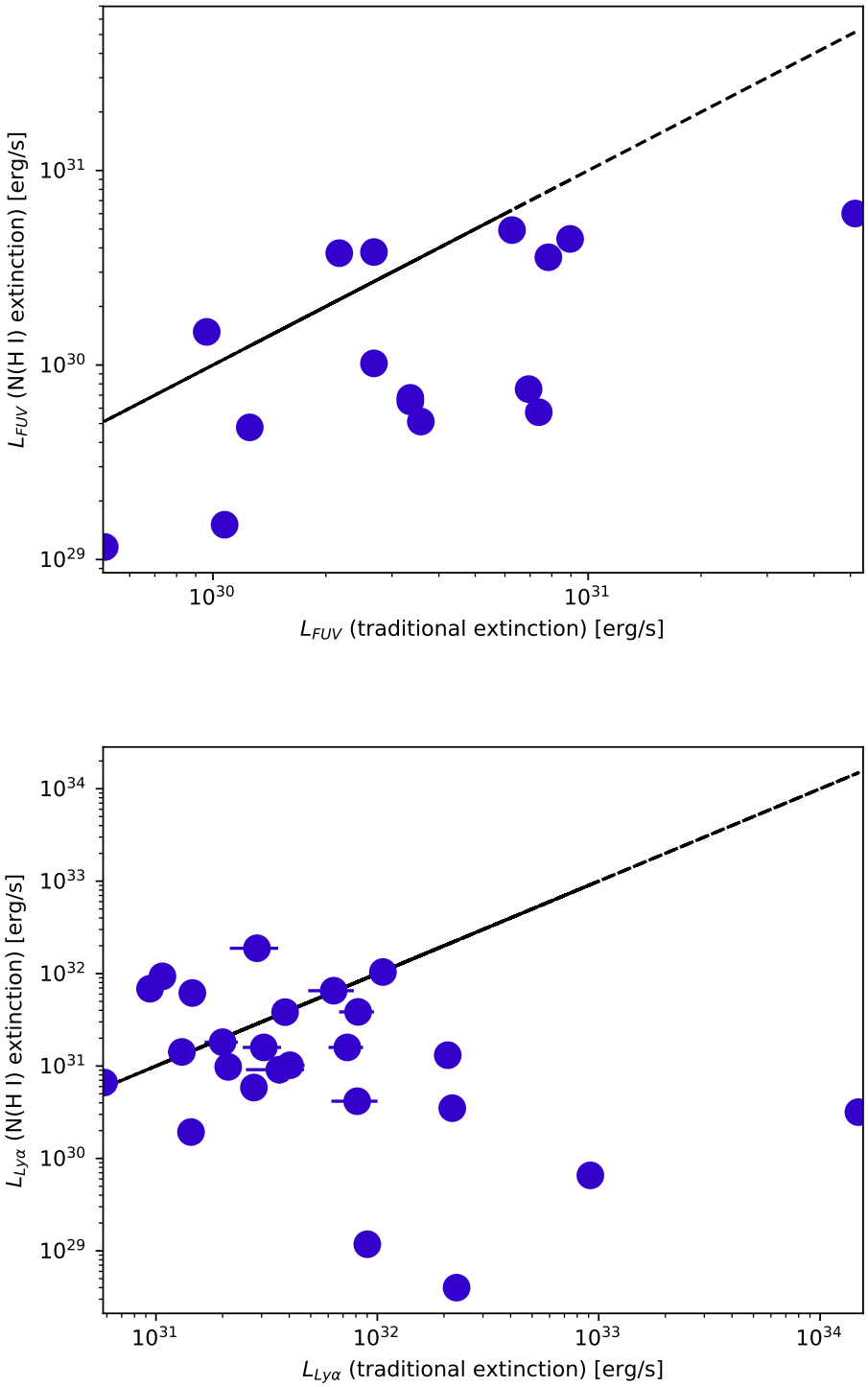

Figure 3: Comparison of luminosities from the FUV continuum (top) and Lyα (bottom), calculated using different values of A_V to deredden the spectrum. The method described in McJunkin et al. (2014), which uses the Lyα wings to estimate $N\,(HI)$ along the line of sight, typically yields smaller A_V and lower luminosities than more traditional methods (1-to-1 relationship traced by black, dashed lines). Since the $N\,(HI)$-based measurements alleviate the correlation between A_V and total flux from UV-H_2 (France et al. 2017), we adopt those extinctions for the analysis presented here.

Gómez de Castro, A. I., & Ferro-Fontán, C. 2005, MNRAS, 362, 569
Green, J. C., et al. 2012, ApJ, 744, 60
Guilloteau, S., Di Folco, E., Dutrey, A., Simon, M., Grosso, N., & Piétu, V. 2013, A&A, 549, A92
Hartigan, P., & Kenyon, S. J. 2003, ApJ, 583, 334
Henning, T., et al. 2010, ApJ, 714, 1511
Herczeg, G. J., Linsky, J. L., Valenti, J. A., Johns-Krull, C. M., & Wood, B. E. 2002, ApJ, 572, 310
Herczeg, G. J., et al. 2005, AJ, 129, 2777
Herczeg, G. J., Wood, B. E., Linsky, J. L., Valenti, J. A., & Johns-Krull, C. M. 2004, ApJ, 607, 369
Hoadley, K., France, K., Alexander, R. D., McJunkin, M., & Schneider, P. C. 2015, ApJ, 812, 41
Houck, J. R., et al. 2004, ApJS, 154, 18
Huang, J., et al. 2018, ApJL, 869, L42
Johns-Krull, C. M., & Herczeg, G. J. 2007, ApJ, 655, 345
Kenyon, S. J., & Hartmann, L. 1995, ApJS, 101, 117
Kurtovic, N. T., et al. 2018, ApJL, 869, L44
Lebouteiller, V., Barry, D. J., Goes, C., Sloan, G. C., Spoon, H. W. W., Weedman, D. W., Bernard-Salas, J., & Houck, J. R. 2015, The Astrophysical Journal Supplement Series, 218, 21
Lebouteiller, V., Barry, D. J., Spoon, H. W. W., Bernard-Salas, J., Sloan, G. C., Houck, J. R., & Weedman, D. W. 2011, ApJS, 196, 8
Li, X., Heays, A. N., Visser, R., Ubachs, W., Lewis, B. R., Gibson, S. T., & van Dishoeck, E. F. 2013, A&A, 555, A14
Madhusudhan, N., Mousis, O., Johnson, T. V., & Lunine, J. I. 2011, ApJ, 743, 191
Manset, N., Bastien, P., Ménard, F., Bertout, C., Le van Suu, A., & Boivin, L. 2009, A&A, 499, 137
McJunkin, M., France, K., Schneider, P. C., Herczeg, G. J., Brown, A., Hillenbrand, L., Schindhelm, E., & Edwards, S. 2014, ApJ, 780, 150
Miotello, A., et al. 2019, arXiv e-prints
—. 2017, A&A, 599, A113
Najita, J. R., Carr, J. S., Pontoppidan, K. M., Salyk, C., van Dishoeck, E. F., & Blake, G. A. 2013, ApJ, 766, 134
Nuth, J. A., & Glicker, S. 1982, JQSRT, 28, 223
Öberg, K. I., Boogert, A. C. A., Pontoppidan, K. M., Blake, G. A., Evans, N. J., Lahuis, F., & van Dishoeck, E. F. 2008, ApJ, 678, 1032
Öberg, K. I., et al. 2011, ApJ, 734, 98
Pascucci, I., Apai, D., Luhman, K., Henning, T., Bouwman, J., Meyer, M. R., Lahuis, F., & Natta, A. 2009, ApJ, 696, 143
Pascucci, I., Herczeg, G., Carr, J. S., & Bruderer, S. 2013, ApJ, 779, 178
Pontoppidan, K. M., Salyk, C., Blake, G. A., Meijerink, R., Carr, J. S., & Najita, J. 2010, ApJ, 720, 887
Salyk, C., Blake, G. A., Boogert, A. C. A., & Brown, J. M. 2011a, ApJ, 743, 112
Salyk, C., Pontoppidan, K. M., Blake, G. A., Najita, J. R., & Carr, J. S. 2011b, ApJ, 731, 130
Schindhelm, E., France, K., Burgh, E. B., Herczeg, G. J., Green, J. C., Brown, A., Brown, J. M., & Valenti, J. A. 2012a, ApJ, 746, 97
Schindhelm, E., et al. 2012b, ApJL, 756, L23
Schwarz, K. R., Bergin, E. A., Cleeves, L. I., Zhang, K., Öberg, K. I., Blake, G. A., & Anderson, D. 2018, ApJ, 856, 85
Simon, M. N., Pascucci, I., Edwards, S., Feng, W., Gorti, U., Hollenbach, D., Rigliaco, E., & Keane, J. T. 2016, ApJ, 831, 169
Tazzari, M., et al. 2017, A&A, 606, A88
The Astropy Collaboration et al. 2018, ArXiv e-prints
van der Marel, N., et al. 2018, ApJ, 854, 177
van Dishoeck, E. F., Jonkheid, B., & van Hemert, M. C. 2006, Faraday Discussions, 133, 231
van Terwisga, S. E., et al. 2019, A&A, 623, A150
Visser, R., Bruderer, S., Cazzoletti, P., Facchini, S., Heays, A. N., & van Dishoeck, E. F. 2018, A&A, 615, A75
Walsh, C., Nomura, H., Millar, T. J., & Aikawa, Y. 2012, ApJ, 747, 114
Walsh, C., Nomura, H., & van Dishoeck, E. 2015, A&A, 582, A88
Woodgate, B., et al. 1997a, in Bulletin of the American Astronomical Society, Vol. 29, American Astronomical Society Meeting Abstracts #190, 836
Woodgate, B. E., et al. 1997b, in Proc. SPIE, Vol. 3118, Imaging Spectrometry III, ed. M. R. Descour & S. S. Shen, 2–12
Yang, H., et al. 2012, ApJ, 744, 121

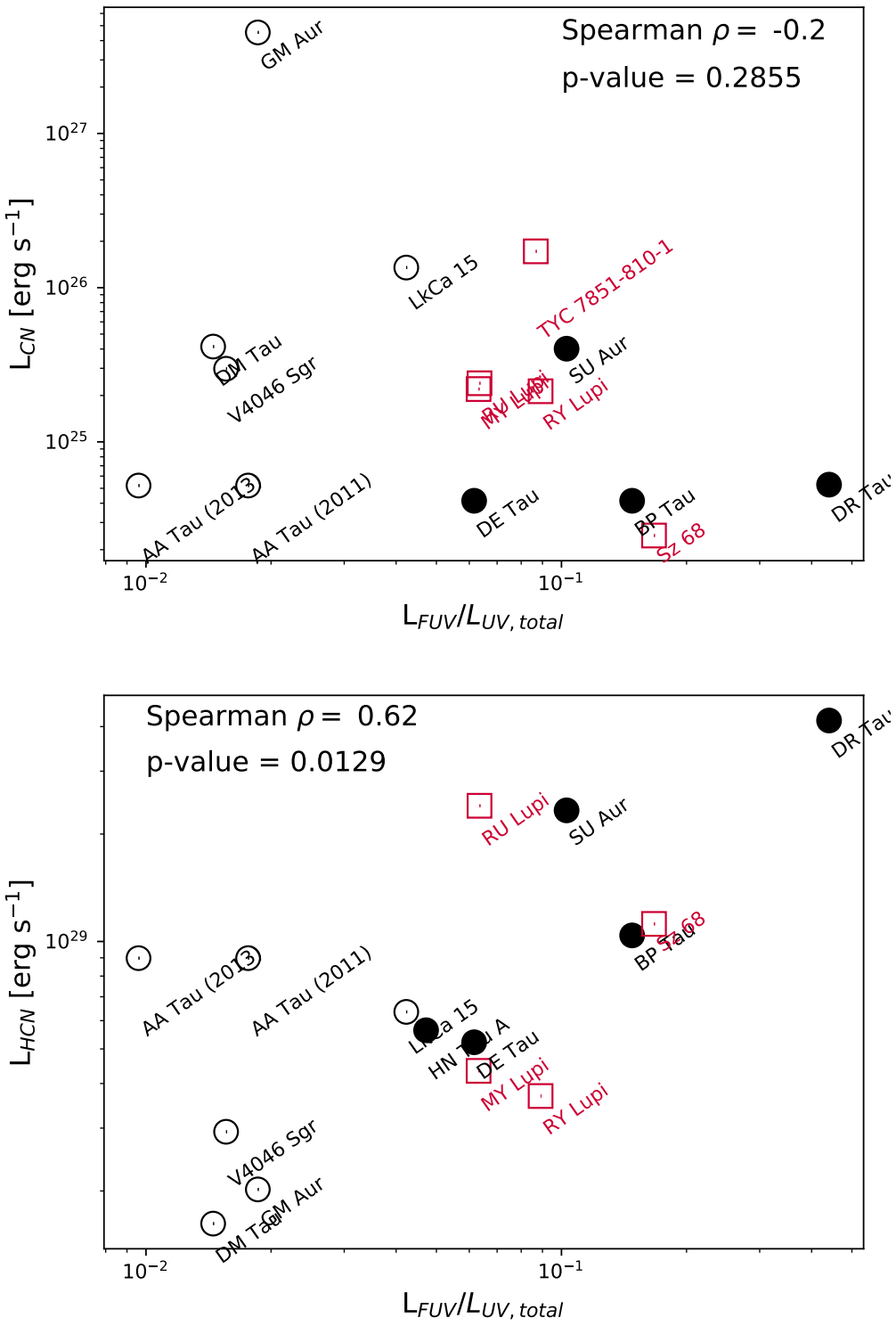

Figure 5: Relative flux from the FUV continuum (integrated from 912-1650 Å) versus sub-mm CN (top) and 14 μm HCN (bottom) luminosities. The five Lupus systems are shown as red squares and the subset of disks from France et al. (2017) as black circles, with open markers representing disks with resolved dust substructure. N_2 molecules are readily predissociated by photons between 912-1000 Å(Li et al. 2013), and the atomic nitrogen then reacts with H_2^* as a first step in CN formation (Walsh et al. 2015; Cazzoletti et al. 2018). The positive correlation between HCN and FUV continuum emission demonstrates that N_2 photodissociation may proceed more efficiently in disks that are more strongly irradiated by FUV photons relative to the rest of the UV spectrum.

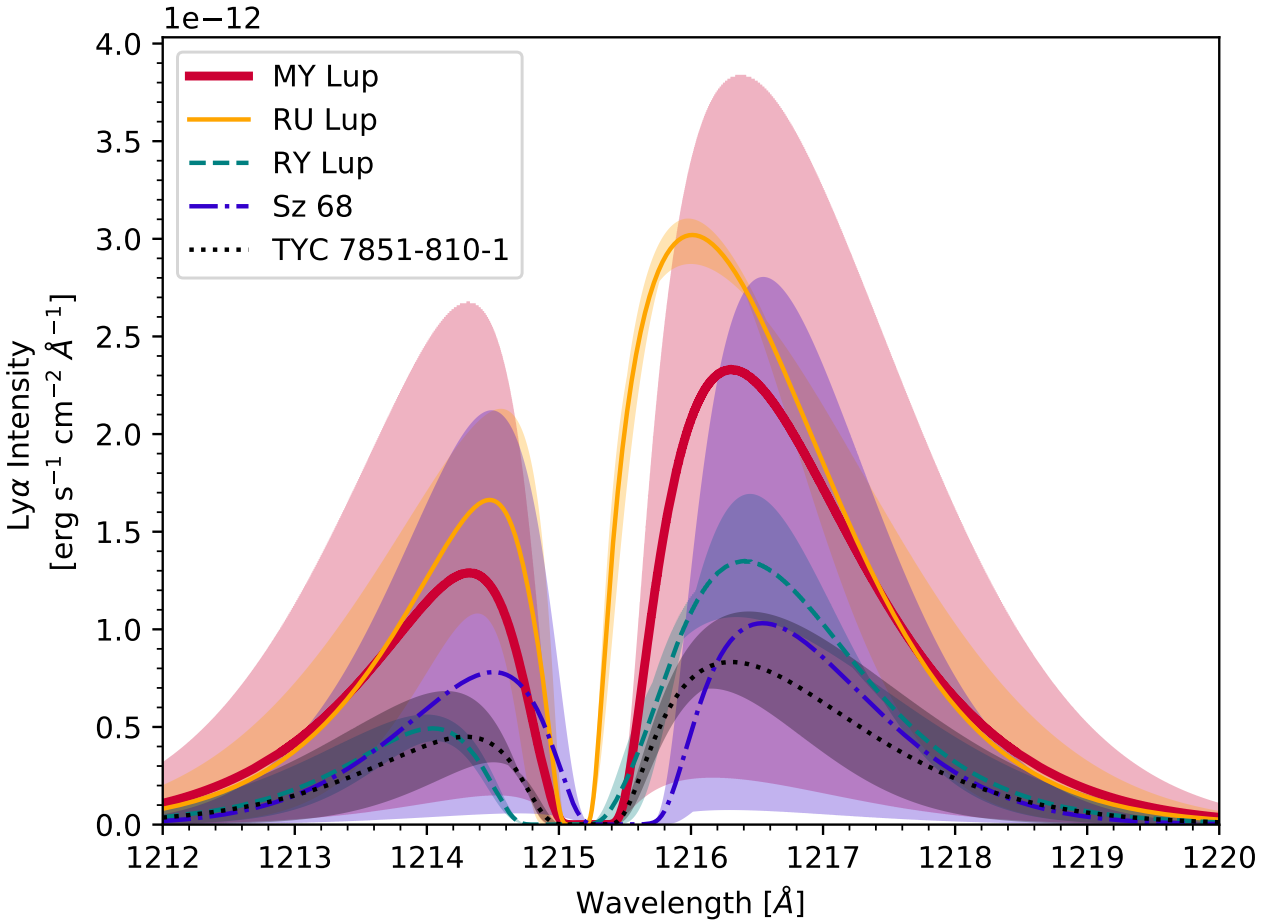

Figure 6: A comparison of the reconstructed Lyα profiles for all five Lupus targets in our sample, with colored contours showing rough uncertainties associated with the modeling process. The reconstruction is done using observed UV-H_2 emission lines as data points (Schindhelm et al. 2012b), since molecules are pumped into these excited electronic states by Lyα photons.

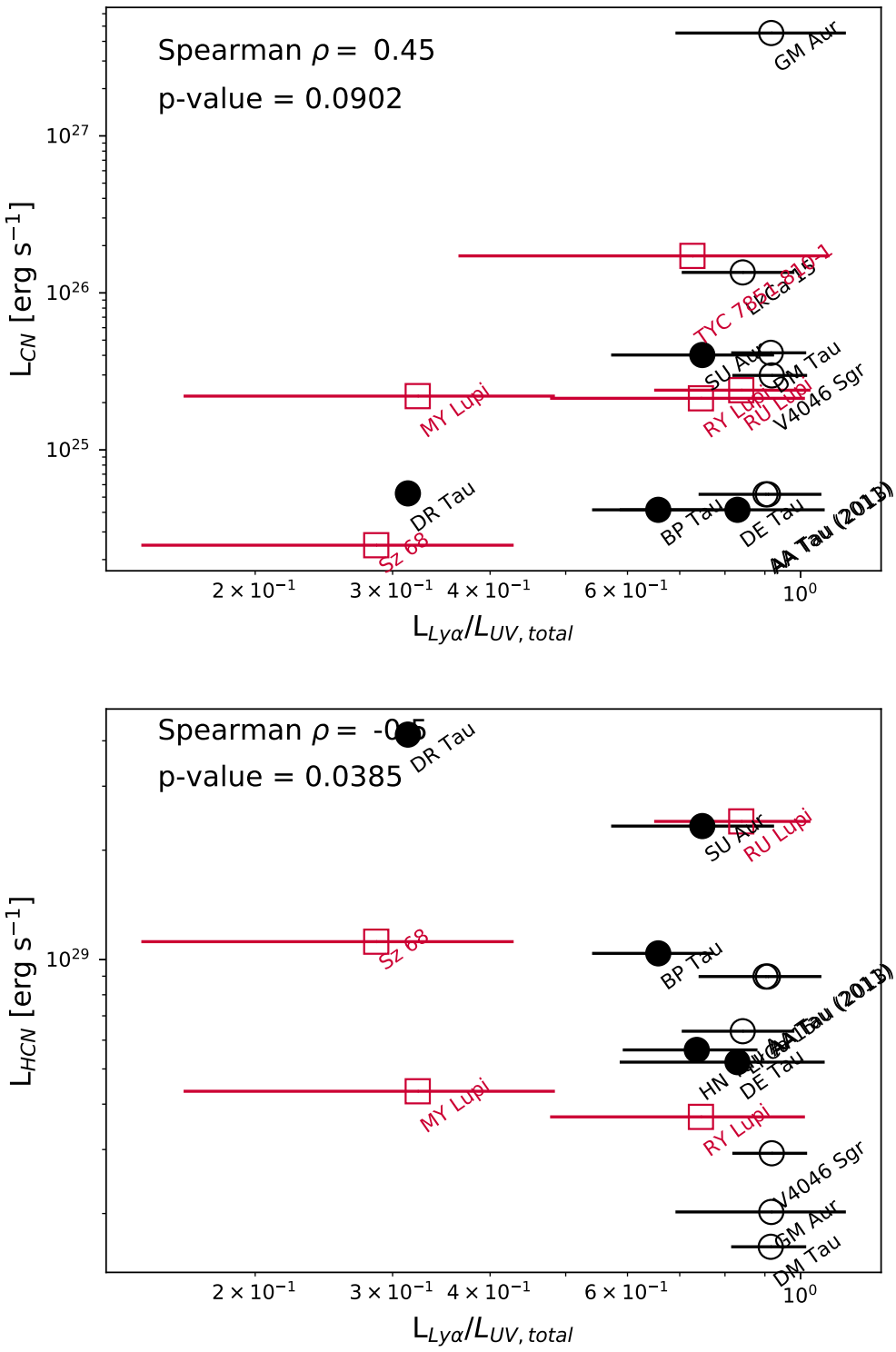

Figure 8: Relative Lyα luminosity versus sub-mm CN (top) and 14 μm HCN (bottom) emission. The Lupus disks are shown as red squares and systems from France et al. (2017) as black circles, with open markers representing systems with resolved dust substructure. CN and Lyα are uncorrelated, but we find a significant negative correlation between HCN and Lyα. This result demonstrates that HCN is more readily photodissociated in systems with stronger Lyα emission relative to the rest of the UV spectrum, although we note that the relationship is strongly influenced by DR Tau.

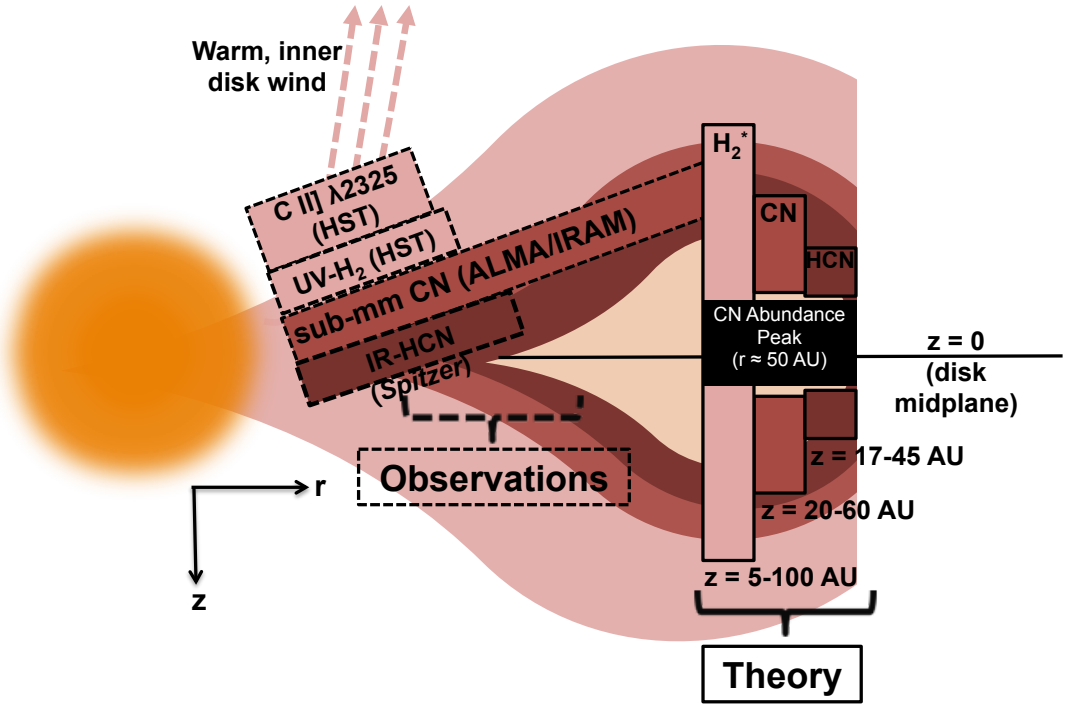

Figure 9: Rough spatial locations of emitting gas that produces C II] λ2325, UV-H_2, IR-HCN, and sub-mm-CN emission lines, compared to radius where physical-chemical models predict peak abundances of H_2^*, CN, and HCN (Cazzoletti et al. 2018). The observed gas populations should overlap at radii close to the central star, although the sub-mm CN emission is the only component that generally extends across the full disk.

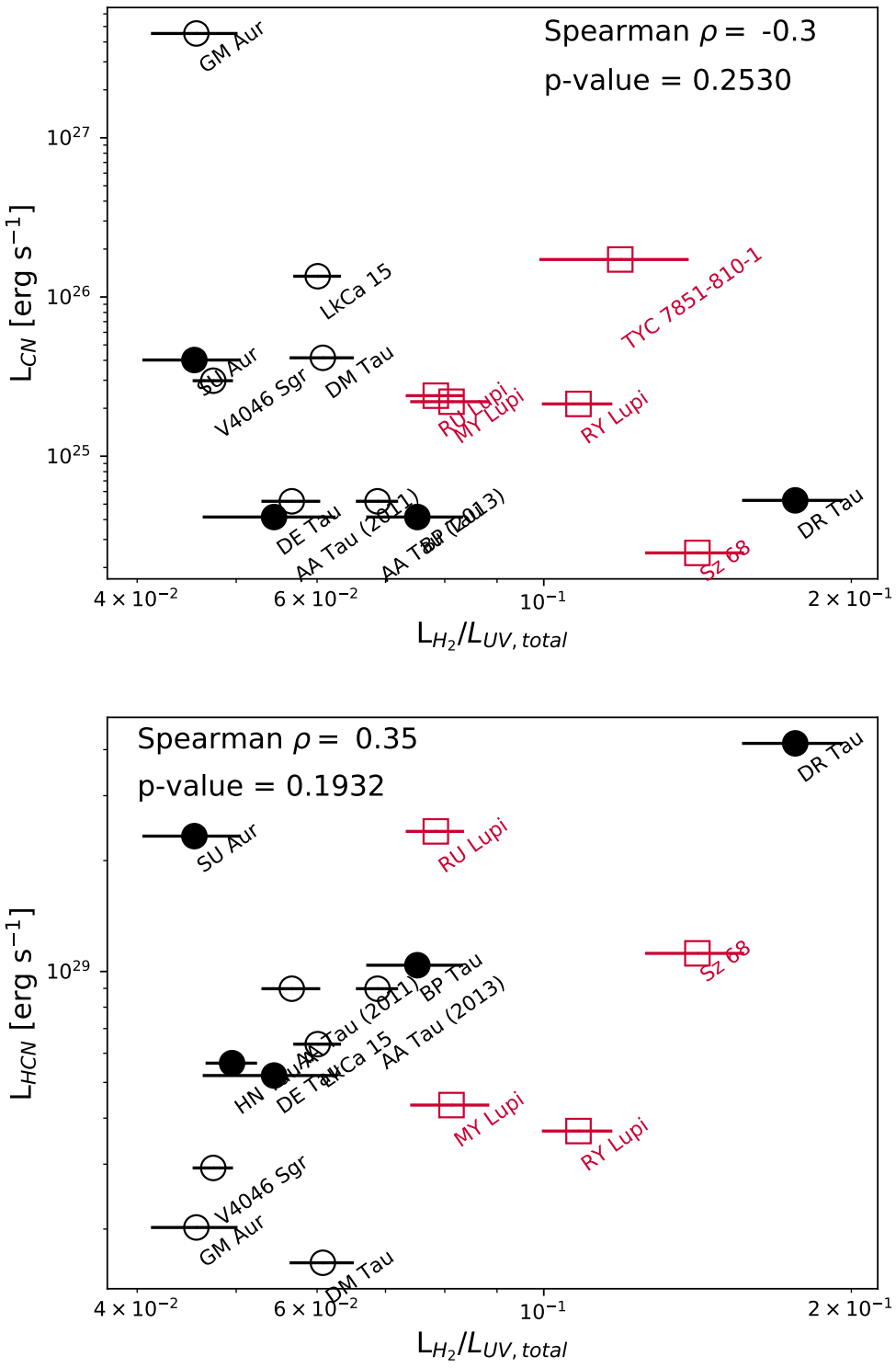

Figure 11: Total luminosity from UV-pumped H_2 versus CN and HCN luminosities, with open markers representing disks with resolved dust substructure (i.e. rings, gaps, or cavities). The Lupus disks are shown as red squares, while the black circles are systems from France et al. (2017). Neither sub-mm CN or IR HCN is significantly correlated with UV-H_2, which is likely due to the disparate radial and vertical stratification of the three populations of emitting gas.

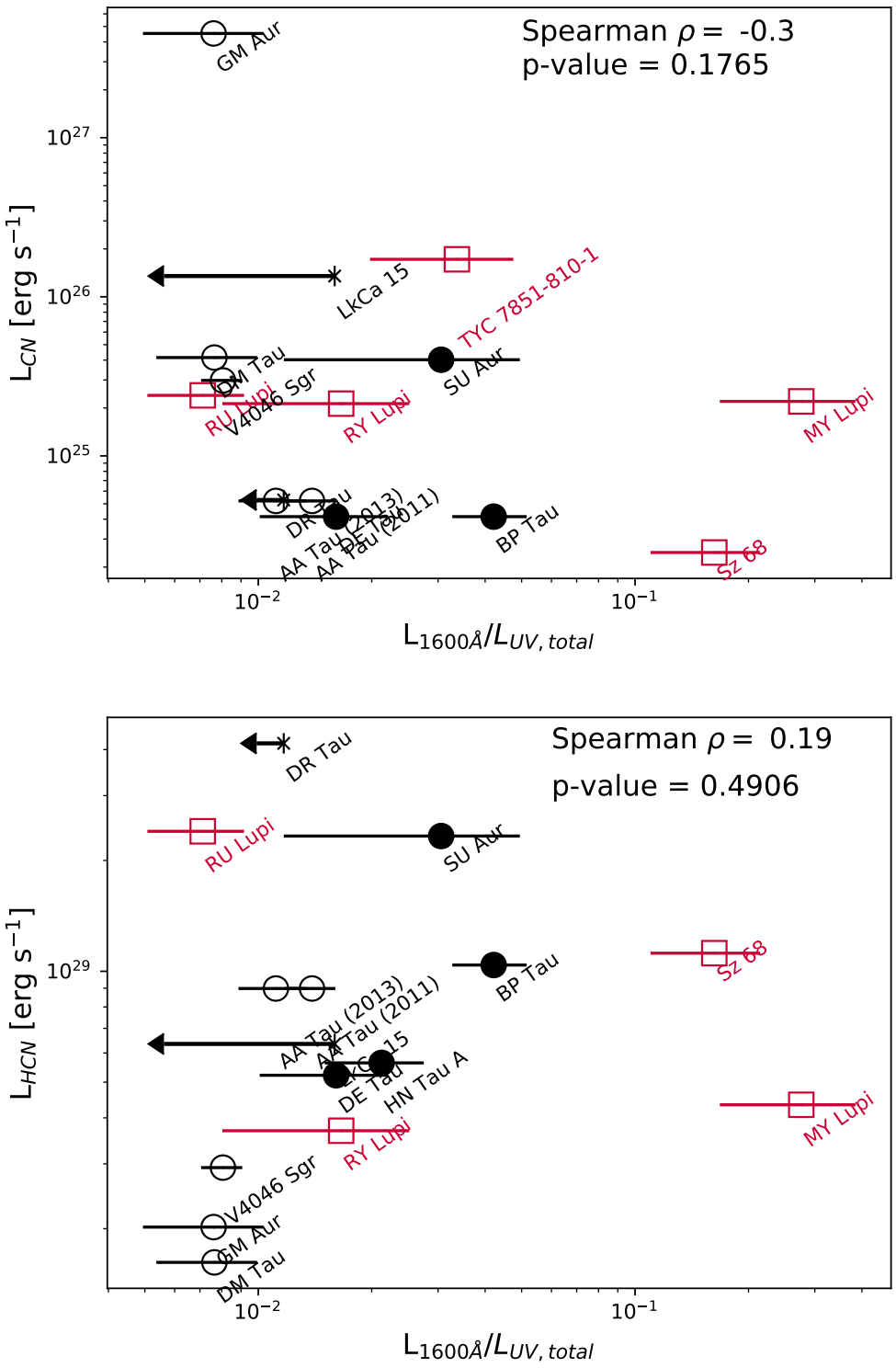

Figure 13: Total luminosity from the 1600 Å bump (produced by H_2^* produced during H_2O photodissociation; France et al. 2017) versus CN and HCN luminosities. The Lupus disks are shown as red squares, while the black circles are systems from France et al. (2017). The strength of the bump is correlated with time-varying accretion luminosities (Espaillat et al. 2019), implying that the measurements shown here are snapshots of the population of hot, non-thermal gas and not necessarily reflective of equilibrium chemical conditions.

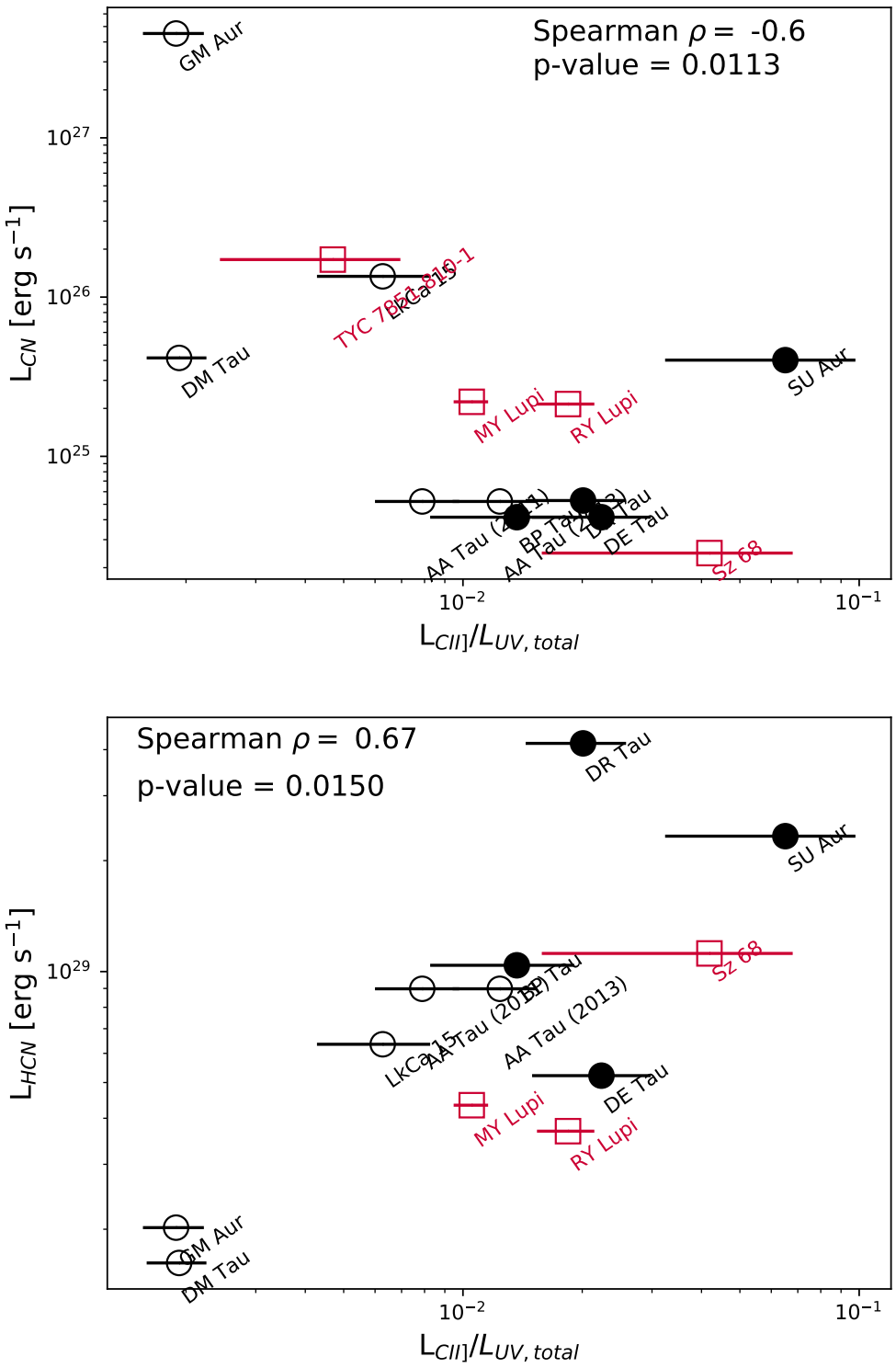

Figure 15: C II] λ2325 versus HCN and CN luminosities. The five Lupus systems are shown as red squares and the subset of disks from France et al. (2017) as black circles, with open markers representing disks with resolved dust substructure. Although the sub-mm CN is uncorrelated with the C II] feature, a strong positive correlation is seen with the IR HCN emission. The relationship can be attributed to either accretion processes that enhance both C II] and HCN emission or molecule formation that proceeds more efficiently with larger abundances of inner disk C^+.

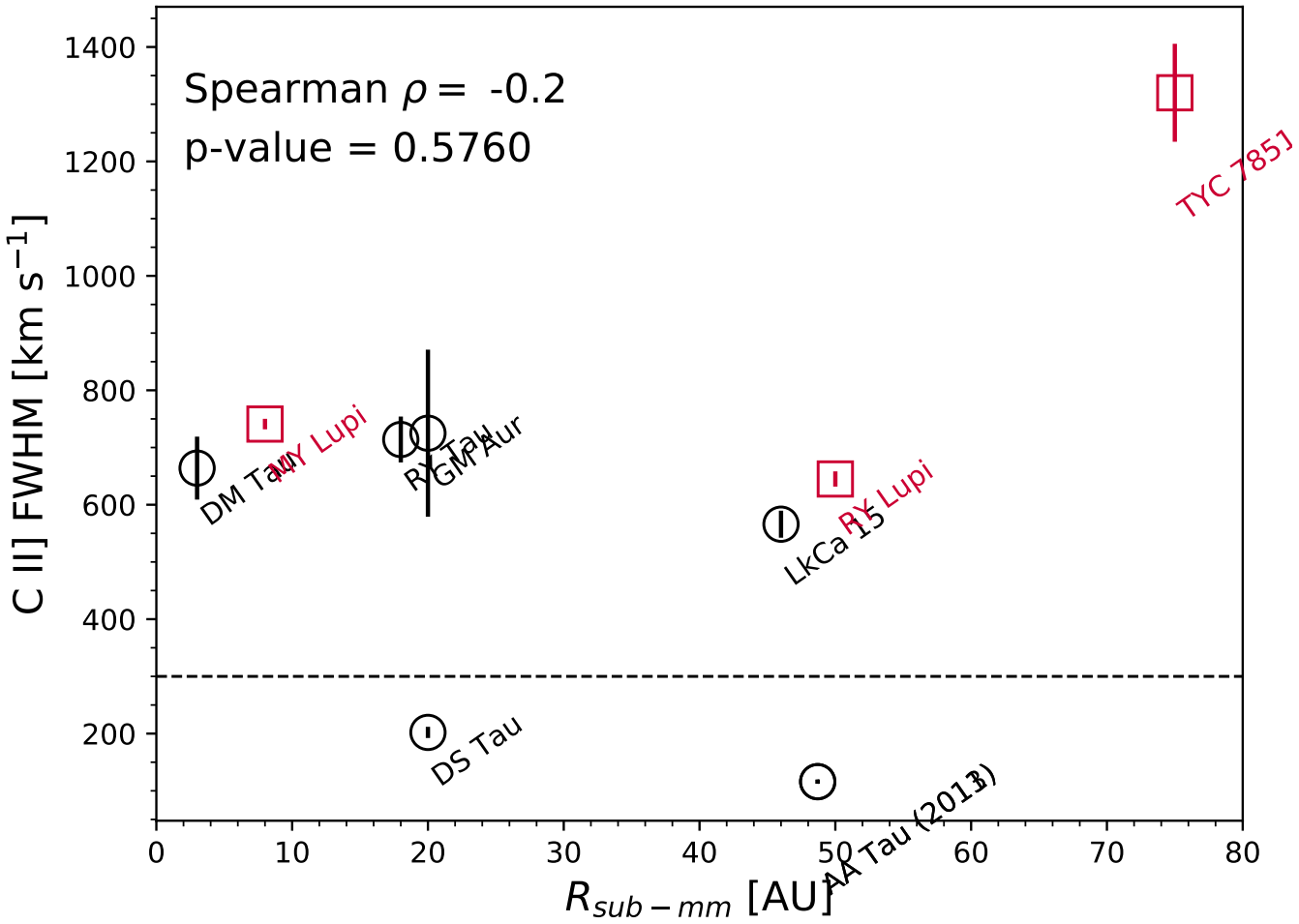

Figure 16: A comparison of the FWHM of C II] λ2325 emission lines and the innermost radii of sub-mm emission for the disks with resolved dust substructure in our sample. The dashed line represents the instrument resolution of the G230L grating on *HST*-STIS at these wavelengths. Observations of DS Tau and AA Tau were acquired with the higher-resolution ($R \sim 30,000$) E230M grating. We find no clear relationship between the C II] line widths and dust substructure location, making it difficult to confirm the exact spatial location of the population of emitting C^+.

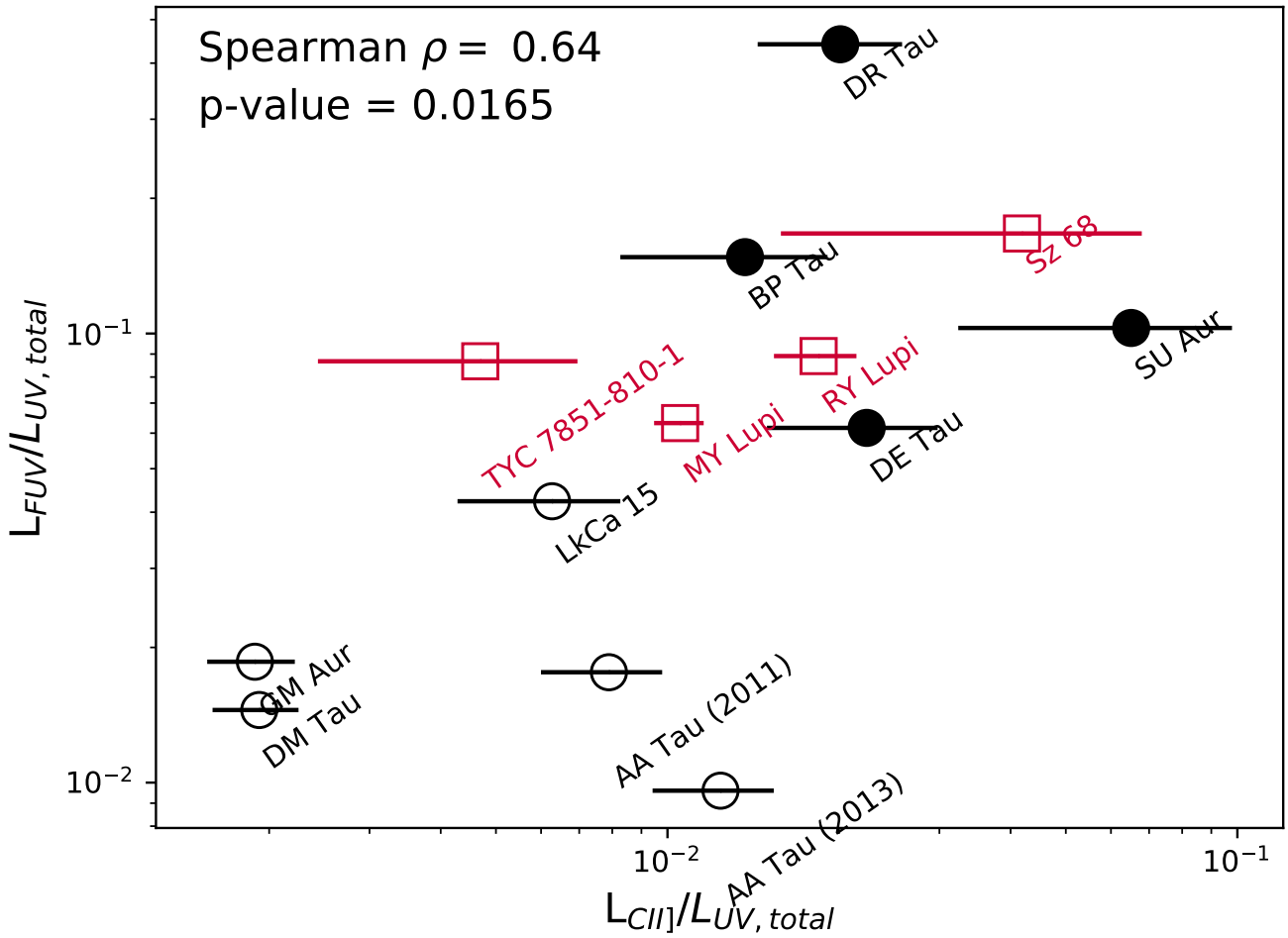

Figure 17: Fractional luminosities of C II] λ2325 and FUV continuum emission. Both quantities are significantly correlated with 14 μm HCN emission, implying that systems with stronger FUV and C II] fluxes are better able to produce HCN in the inner disk. A full kinematic analysis of the C II] line profiles is likely required to determine whether the C II] emission traces the C^+ population involved in gas-phase chemistry or accretion processes that enhance the strength of the feature.

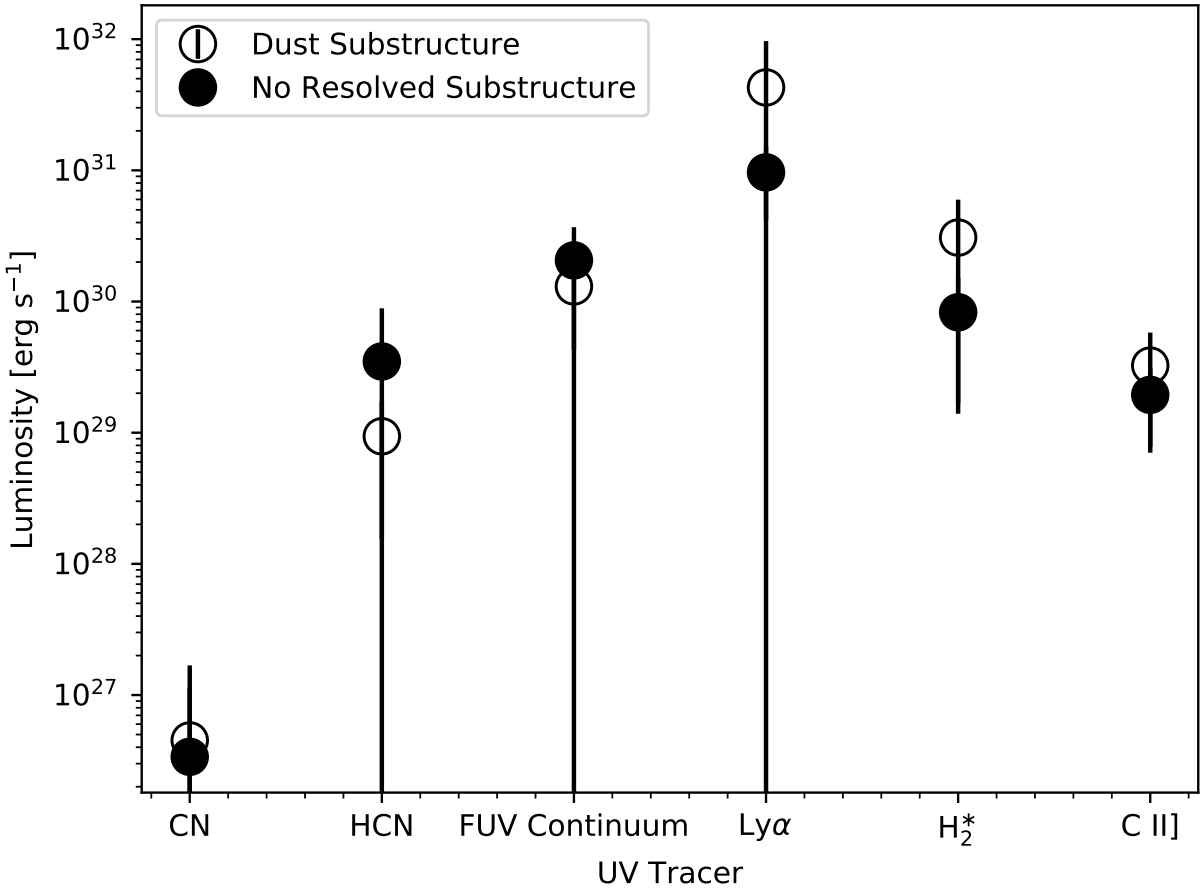

Figure 18: A comparison of the average properties of disks with resolved dust substructure (open circles) and full primordial disks (filled circles). We tentatively find that emission from CN, Lyα, UV-H_2, and C II] λ2325 are stronger in more evolved disks, while HCN and FUV continuum emission are stronger in primordial disks. However, the sample sizes of the two groups are too small to draw significant conclusions at this time.

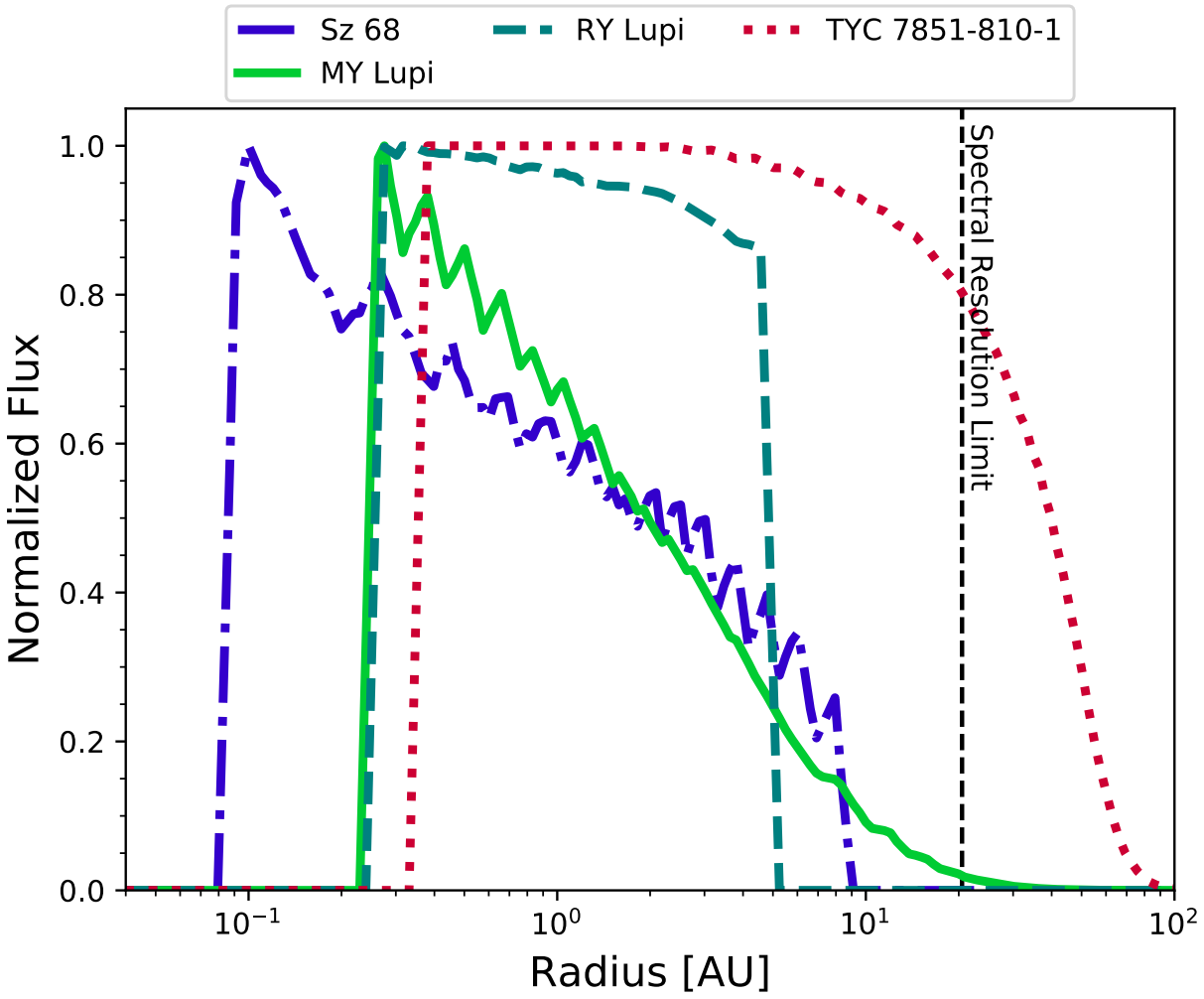

Figure 19: Radial distributions of flux from hot, UV-fluorescent H_2 in 4/5 of the Lupus disks presented here, obtained by fitting a 2-D radiative transfer code to individual emission lines. Features from RU Lupi were not modeled, since many of the UV-H_2 emission lines are asymmetric and show significant blue-shifted excess (Herczeg et al. 2005). The flux distribution in J16083070 extends to much more distant radii than the other three systems, consistent with a depletion of small dust grains inside a large sub-mm cavity ($r_{cav} \sim 75$ AU; van der Marel et al. 2018) that allows Lyα photons to travel further into the gas disk. Although the flux distribution from MY Lupi spans the radii of its first two dust rings ($r \sim 8, 20$ AU; Huang et al. 2018), we detect no sign of a break in the population of hot gas. Finally, we note that the flux distribution from Sz 68 is sharply truncated around 10 AU, implying that the UV-H_2 emission extends to the edge of the system's circumprimary disk (Kurtovic et al. 2018).

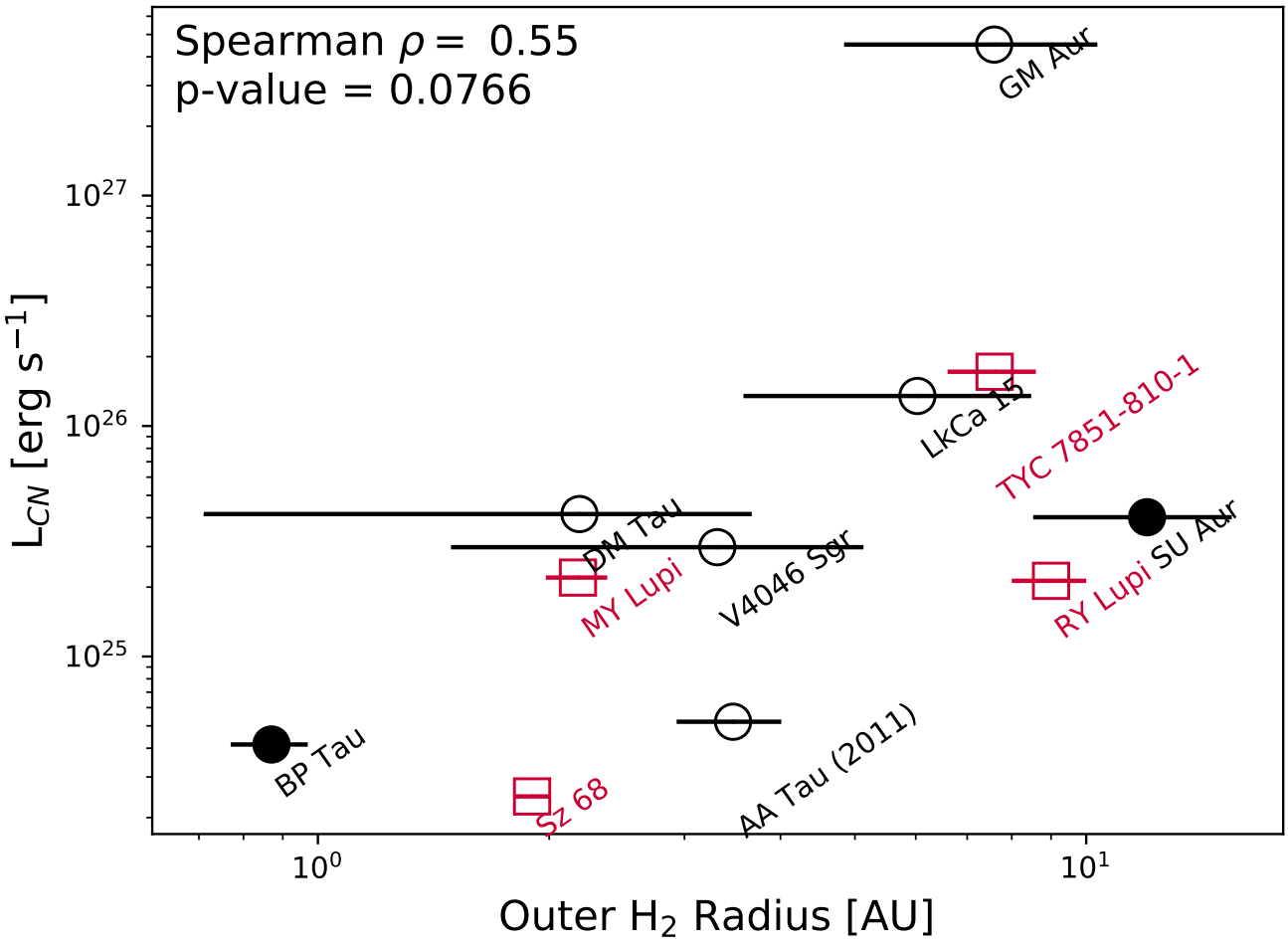

Figure 20: Outer radius of UV-H_2 emission vs. sub-mm CN luminosity. 2-D radiative transfer models were used to reproduce the underlying radial distribution of flux that best reproduces the observed UV-H_2 emission lines, with the outer radius representing the location within which 95% of the flux is contained. The black markers represents systems that were modeled by Hoadley et al. (2015), while the red markers are disks that were modeled in Arulanantham et al. (2018) and this work. Although not a statistically significant correlation, the observed trend tentatively demonstrates that more CN molecules are produced in disks that are more optically thin to the Lyα photons responsible for pumping H_2^* into excited electronic states.

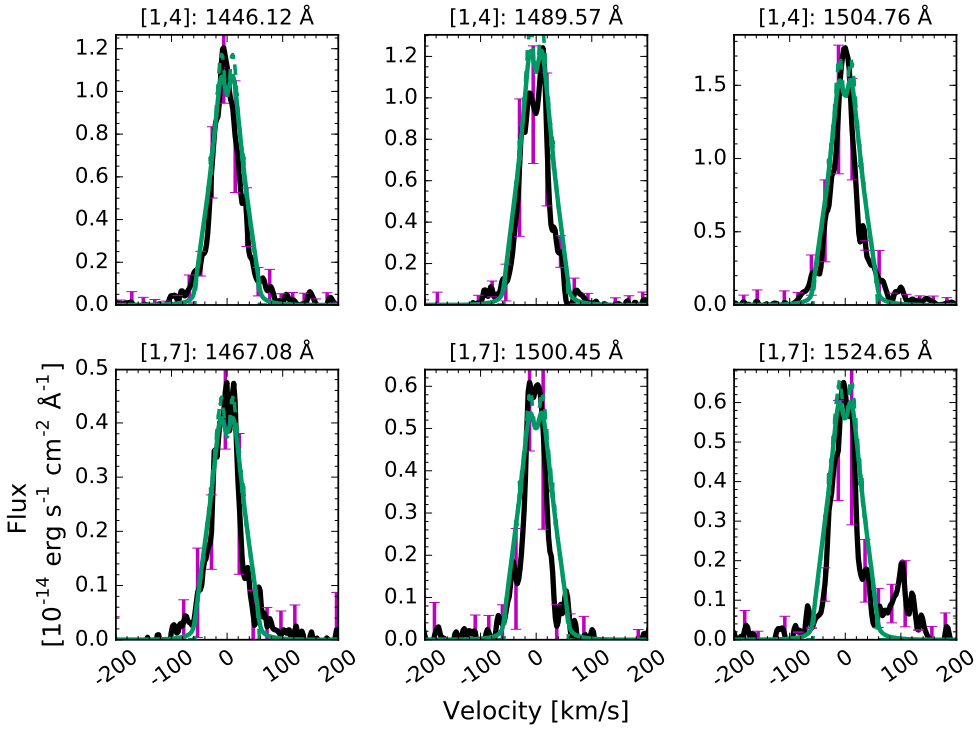

Figure A.1: Observed UV-H_2 emission lines (black) and model distributions (teal) for MY Lupi

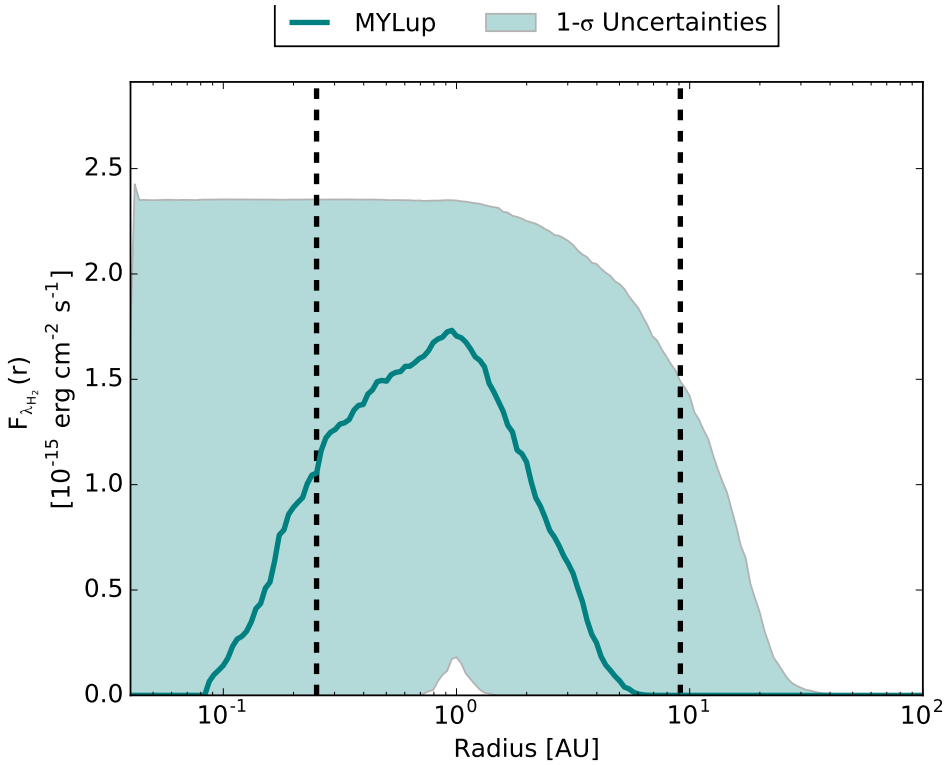

Figure A.2: Model radial distribution of UV-H_2 flux from the disk around MY Lupi, with contours marking $+/-1\sigma$ bounds

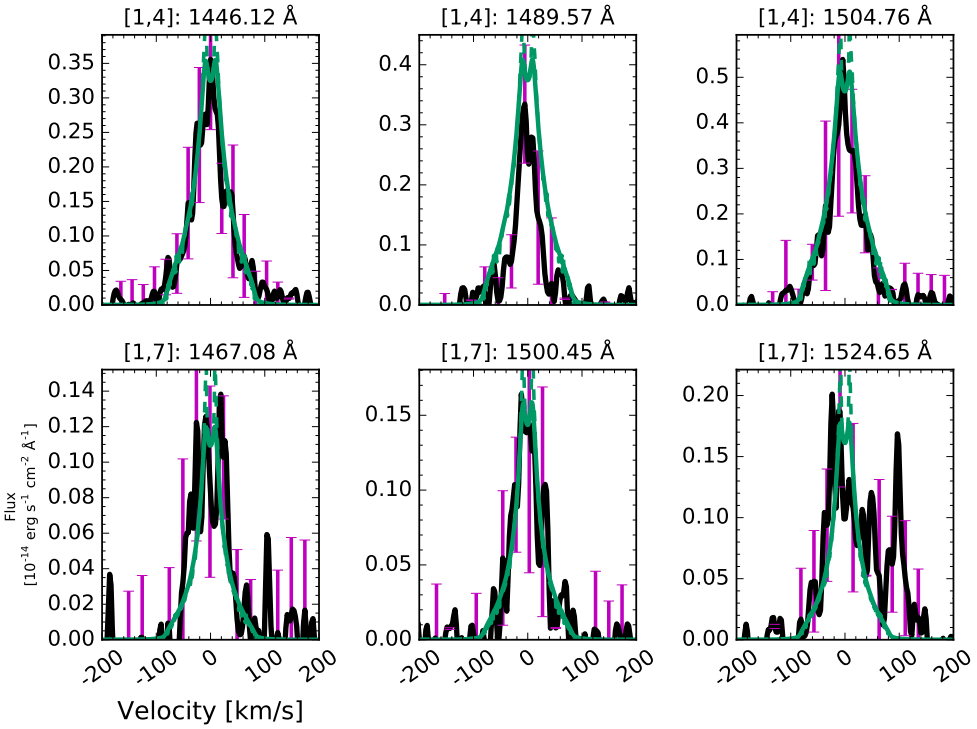

Figure A.3: Observed UV-H_2 emission lines (black) and model distributions (teal) for Sz 68

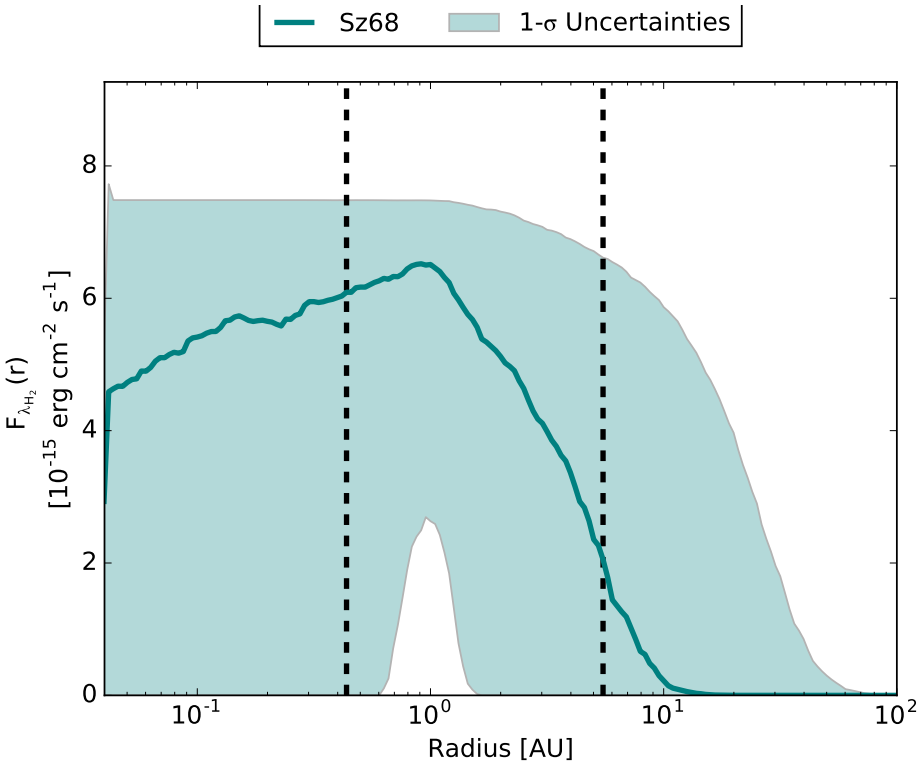

Figure A.4: Model radial distribution of UV-H_2 flux from the disk around Sz 68, with contours marking $+/-1\sigma$ bounds

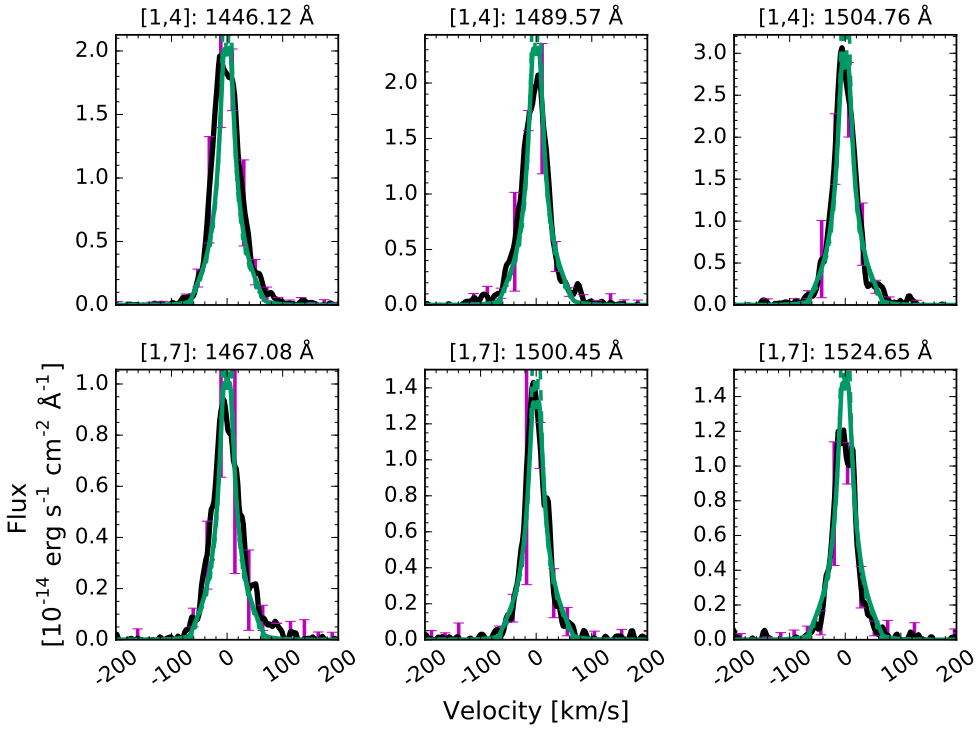

Figure A.5: Observed UV-H_2 emission lines (black) and model distributions (teal) for J16083070

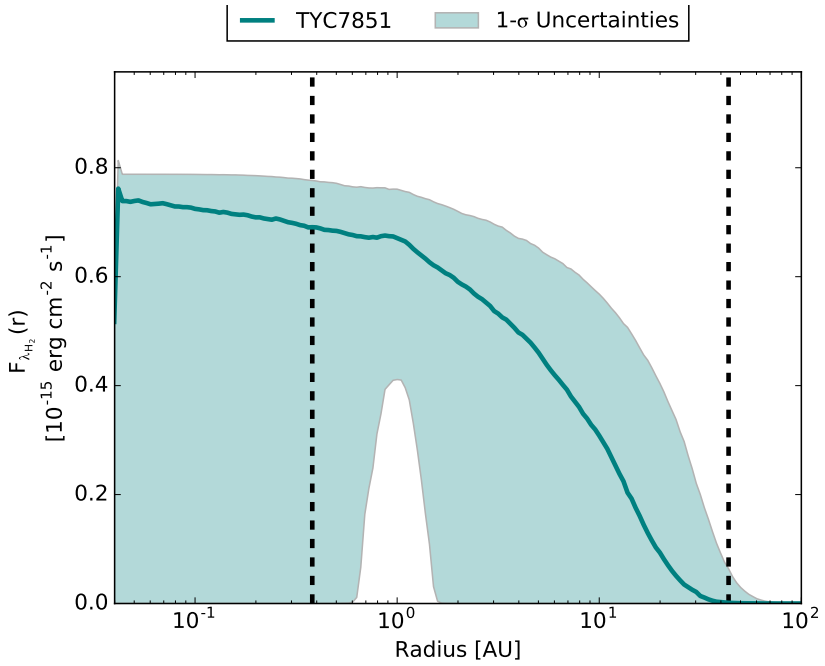

Figure A.6: Model radial distribution of UV-H_2 flux from the disk around J16083070, with contours marking $+/-1\sigma$ bounds.